VRIJE UNIVERSITEIT BRUSSEL

Brussels - Belgium

&

UNIVERSIDADE DO PORTO

Porto - Portugal

# HOE Aberration Correction with an Intermediate CGH

José Figueiredo

**Project Report**

This project was completed under the ERASMUS PROGRAMME at the Vrije Universiteit Brussel (V.U.B.), with the Supervision of Eng. S. Roose 02/05-31/07, 1991

VRIJE UNIVERSITEIT BRUSSEL

Brussels - Belgium

&

UNIVERSIDADE DO PORTO

Porto - Portugal

# HOE Aberration Correction with an Intermediate CGH

**Project Report**

José Maria Longras Figueiredo,

Final Year Student Physics (Optics & Electronics) at the Faculty of Science, University of Porto.

Supervision: Eng. S. Roose (V.U.B)

This work was completed under the ERASMUS PROGRAMME at the Vrije Universiteit Brussel (V.U.B.), under Supervision of Eng. S. Roose.

02/05-31/07, 1991

*Sumário*

Os Elementos Ópticos Holográficos introduzem aberrações nas imagens por eles formadas devido à não correspondência entre a onda de referência e a onda de leitura, ou deformação da onda holográfica É feito um estudo das aberrações dos elementos holograficos. Estas aberrações podem ser atenuadas usando como referência uma onda não-esferica. São usados Hologramas Gerados por Computador na obtenção destas ondas não-esféricas.

*Abstract*

Holographic optical elements (HOEs) have shown potential as a viable supplement to classic refractive optics. This work discusses the problem of mismatch between the reference and reconstruction beams that introduces aberration in the images. It is discussed a method to attenuate the aberration. This methods uses a CGH as a wave transformer.

***"Valeu a pena ? Tudo vale a pena***
***Se a alma não é pequena."***

*"Was it worth while ? It is worth while, all,*

*If the soul is not small."*

Fernando Pessoa
Lisboa, 1888-1935


## *Acknowledgments*

I thank Prof. Irina Veretennicoff and Prof. Olivério Soares, promotors of the ERASMUS PROGRAMME at the Vrije Universiteit Brussel and at the Universidade do Porto, respectively. My special gratitude to Prof. Irina, who received me in her laboratory.

I also thank all the people at VUB that welcome me, specially Prof. Erik Stijns.

Thanks also to my colleagues ERASMUS students Hervé DUPONT and Olivier ROUSSEL-GALLE, for the way they received me in the "ERASMUS House", and for their friendship.

Finally I want to thank Eng. Steve Roose, supervisor of my work at VUB, for his support and attention.

# Contents

# Introduction

An optical system can be thought as an arrangement of devices that transforms input wavefronts into output wavefronts. Until some years ago most practical optical systems were composed of refractive (lenses) and reflective (mirrors) elements.

The class of transformations that links the output wavefronts to the input wavefronts in refractive-reflective optical systems is limited. For example, it is not possible to design a refractive-reflective optical system for which the output wavefront is a three-dimensional image of a three-dimensional object when the input wavefront is a collimated beam.

This particular input-output transformation can, however, be realized by using a hologram. When holograms are employed as the transfer function element in optical systems, they are refered to as Holographic Optical Elements (HOEs)[1,2,3,4,5,6].

If an optical system is used with monochromatic light (ideally single wavelength light, but in practice with a small spread of wavelengths from $\lambda$ to $\lambda+\Delta\lambda$ where $\Delta\lambda << \lambda$), it should give a point image conjugate to a point object, a line image for a line object, and a plane for a plane.

However most practical systems give rise to images which are not corresponding points, lines or planes, i.e., the image presents monochromatic aberrations. These were first investigated by Von Seidel and they are now called the five Seidel Aberrations: Spherical Aberration, Coma, Astigmatism, Field Curvature and Distortion[7].

In general, HOEs present large amounts of aberrations caused by the mismatch of the reference wavefront that is used to record the hologram and the reconstruction wavefront that is used to generate the image[1,8,9,10,11,12,13].

The aim of this work was to try to reduce the monochromatic aberrations that are caused when the reconstruction wavefront does not duplicate the geometry of one of the construction wavefronts, using a Computer-Generated Hologram (CGH). This generates an aspheric wavefront that, added to the reference wavefront used to record the HOE, will permit to compensate the aberrations caused by that mismatch'[3,14,15]'.

In this work, CGHs were exploited for generating the recording aberrated waves, and not for the generation of the final HOE, because the printer device avaliable did not have the necessary Space Bandwidth Product (SBWP)'[16,17]'.

This work started last year with the study and the definition of the parameters related to HOE aberrations, followed by the design of the CGH with the desired wavefront'[18]'.

After this phase, several HOEs were recorded with a reference wavefront generated by an intermediate CGH'[14,19]'. The next step was the analysis of different HOE's recorded with this method, and the comparison with uncorrected HOEs.

This report is divided in three parts. In the first part, the background and calculations necessary for the implementation of the CGH wavefronts are presented. In the second part, different set-ups used to analysis the fidelity of CGHs, to record HOEs and to analyse of the non-corrected HOEs and corrected HOEs are presented. In the third part, the results obtained presented and discussed .

# List of acronyms

Articleson Computer-Generated Holography and Holographic Optical Elements contain many acronyms; some of them are used in this report:

| | |
|---|---|
| CGH: | Computer-Generated Hologram (synthetic hologram or digital hologram) |
| OH: | Optical Hologram |
| IOH: | Intermediate Optical Hologram |
| COE: | Classic Optical Element |
| FT: | Fourier Transform |
| FFT: | Fast Fourier Transform |
| HOE: | Holographic Optical Element |
| HL: | Holographic Lens |
| SBWP: | Space Bandwidth Product |
| SNR: | Signal-Noise Ratio |
| VUB: | Vrije Universiteit Brussel |

# Part I: HOEs and CGHs

A1: HOE Characteristics

A2: HOE Aberrations

B1: CG Holography

B2: Realization of a CGH

# A1: HOE Characteristics

## HOE Characteristics[1]

Holographic Optical Elements (HOEs) are optical elements which are recorded by means of interference. They can fulfill similar optical functions to Classic Optical Elements (COEs), such as lenses, mirrors, etc.[1,4].

The optical transfer function of a HOE is based on diffraction phenomena[30,31]. Therefore, the characteristics of these elements will be highly dependent on the hologram spatial structure characteristics, on the hologram construction beams and on the wavelength. Instead, the characteristics of COEs depend basically on the element surface shape. In holography, the shape of the film provides one more degree of freedom in the design of the HOE.

HOEs are useful and sometimes indispensable components of optical systems when the source is monochromatic or when a wavelength-dependent system is desired.

Given an arbitrary input wavefront, a HOE can, in principle, be designed to transform this input wavefront into an arbitrary output wavefront.

Compared to COEs, HOEs are lighter, more compact, and can be formed and replicated easy, and since multiple holograms can be recorded in a single emulsion layer, spatial overlapping of elements is possible.

As a single HOE can often replace several conventional optical elements, one can expect cost reductions for optical systems using HOEs. Examples are holographic scanners for laser printers and robotic vision[23,27].

However, HOEs present a large amounts of aberrations. A comparison between COE and HOE shows that they have similar aberration levels for on-axis configurations, while the off-axis HOEs have four times as much astigmatism and twice as much coma than COEs[1].

In general, the only condition that will elliminate all aberrations simultaneously is to exactly duplicate in the reconstruction process one of the construction wavefronts, or its conjugate. But in many practical situations, such an exact duplication is not possible[8,9,10,11].

These characteristics and their interactions provide both advantages and disadvantages for a particular application.

In general, HOEs will not replace COEs, but will be useful in special, unique applications. Usually, HOEs can be found in optical systems with COEs, operating over a relatively narrow spectral bandwidth.

# A2: HOE Aberrations

## HOEs Aberrations[8,9,10,11,12,13]

In general, a light wave must be represented by a vector function of the position (x,y,z) and time t. There are cases, however, for which such a wave may be adequately described by a scalar function. As our first restriction, we shall consider only monochromatic light waves - waves consisting of a single temporal-frequency component.

The scalar function can be represented by $E(x,y,z,t)=\Psi(x,y,z)EXP(i2\pi\nu qt)$, where $\Psi(x,y,z)$ must satisfy the Helmholtz equation [27]. One solution is the spherical wave, which is described by

$$Q=\frac{A_q}{r_q}EXP[\pm i\frac{2\pi}{\lambda_q}r_q] \qquad [1.a]$$

where $r_q$ is the distance from the point source Q to the point of observation (x,y,z) in the hologram plane, $\lambda_q$ is the wavelength, and $A_q$ is a constant $A_q$, the "$\pm$" indicates a diverging and a converging wave, respectively. The quantity $(\frac{2\pi}{\lambda_q}r_q)$ is called the phase.

In this section, all waves are assumed monochromatic spherical waves originated from point sources and with spatial-dependence described by [1.a].

Consider a hologram recorded with an object wave (O) generated by a point source at coordinates (xo,yo,zo) and a reference wave (R) generated by a point source at coordinates (xr,yr,zr), see fig.1, where the recording film is at plane xy centered at the origin of the coordinate system [30,31].

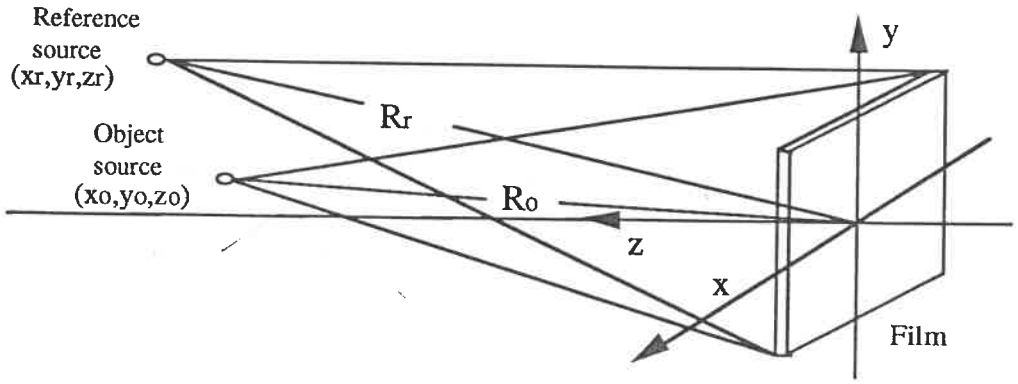


Fig.1. Recording geometry

If the 1/r variation in the fields amplitudes is negligible over the area of the film, we may consider they have constant intensity across the hologram plane. As in our application the wavefronts to be recorded in the holograms have approximately only phase variations, expression [1.a] can by written as

$$Q=A_q \, EXP[\, i\frac{2\pi}{\lambda_q} r_q] \qquad [1.b]$$

The dummy subscript q is replaced by o, r, c, or i, respectively, to denote the object, reference, readout, or image waves.

The total field incident on the photographic film during the recording process is given by:

$$U(x,y)= R(x,y) + O(x,y) \qquad [2]$$

The corresponding intensity distribution across the holographic plane is, thus:

$$\begin{aligned} I(x,y) &= |R|^2 + |O|^2 + RO^* + R^*O \\ &= A_r^2(x,y) + A_o^2(x,y) + 2A_r(x,y)A_r(x,y)\ Cos\ \Phi(x,y) \end{aligned} \qquad [3]$$

where $\Phi(x,y)$ is the phase of the term R*O.

If the amplitude transmittance of the developed film t(x,y) is proportional to the exposure, the terms of interest in the transmittance are

$$t_3 \alpha R^*O \quad \text{and} \quad t_4 \alpha RO^* \qquad [4]$$

When we illuminate the film (after processing) during the reconstruction step, as shown in fig 2, with a spherical wave (C) originating at coordinates (xc,yc,zc), at the output of the transparency two terms related to $t_3$ and $t_4$, are given by

$$H_3(x,y)= C.t_3 \quad \text{and} \quad H_4(x,y)= C.t_4 \qquad [5]$$

Note that the wavelength of the light used during reconstruction ($\lambda_c$) may differ from the wavelength used during the recording process ($\lambda_r$).

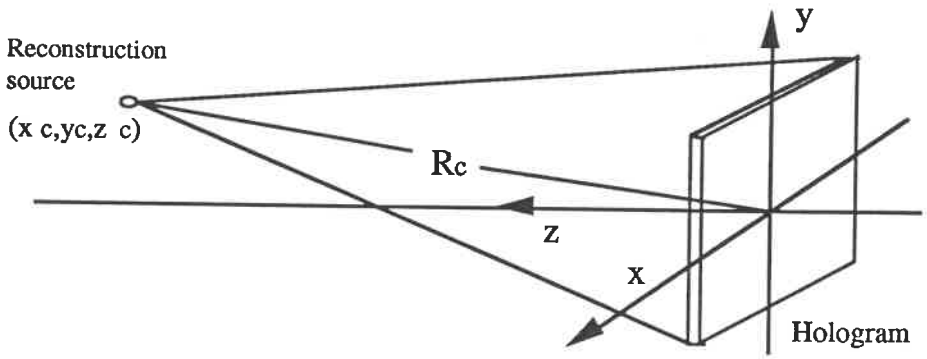


Fig. 2. Reconstruction geometry: reconstruction spherical wave C generated by a point source at coordinates (xc,yc,zc).

The former fields can be written as

$$H_3=A.EXP[i\frac{2\pi}{\lambda c}r_c]\ EXP[i\frac{2\pi}{\lambda r}(r_o-r_r)_m] \qquad [6]$$

and

$$H_4=A.EXP[i\frac{2\pi}{\lambda c}r_c]\ EXP[-i\frac{2\pi}{\lambda r}(r_o-r_r)_m] \qquad [7]$$

The hologram exposed to the readout illumination may be an enlarged copy of the hologram originally recorded; this is denoted by the subscript m on the bracket in [6] and [7]. Throughout this work we assume that the scaling factor m is unity.

To indentify the nature of these transmitted fields, one must examine their (x,y) dependence[8,9,10,11,12,13].

For the purpose of this work it is sufficient to deal only with the phase variation of the participating wavefronts. Thus, their phase at the hologram plane relative to the phase at the origin is given by (fig. 3):

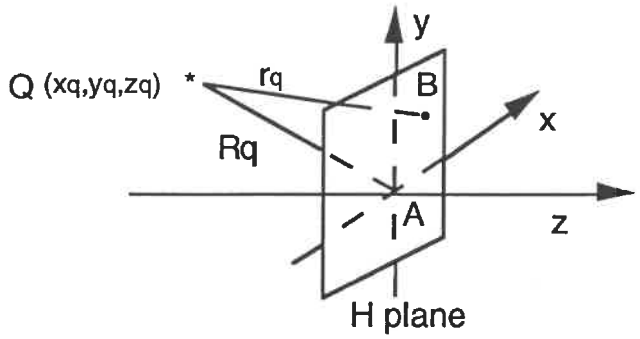


Fig.3. Q wavefront phase at the hologram plane relative to the phase at the origin.

$$\Phi_q(x,y)= \frac{2\pi}{\lambda_j} [QB - QA] \qquad [8]$$

or

$$\Phi_q(x,y)=\frac{2\pi}{\lambda_j} \left\{ \sqrt{(x-xq)^2+(y-yq)^2+zq^2} - \sqrt{xq^2+yq^2+zq^2} \right\} \qquad [9]$$

If $r_q$=[QB - QA] is expanded in a binomial series around Rq, the expansion of the square roots in eq.[9] leads to the following expression for $\Phi_q$:

$$\Phi_q(x,y)=\frac{2\pi}{\lambda q} \left\{ \frac{1}{2Rq} [x^2+y^2-2xxq -2yyq] - \frac{1}{8Rq^3} [(x^2+y^2)^2 - 4(x^2+y^2)(xxq+yyq)+4(xxq+yyq)^2]+... \right\} \qquad [10]$$

where $Rq=\sqrt{xq^2+yq^2+zq^2}$ is the radial distance from the origin to point Q.

There is a need to expand $r_q$=[QB - QA] in a binomial series around Rq and not around Zq, because the binomial expansion of $r_q$ around Rq is less stringent, and it works in situations where the paraxial condition would not be satisfied.

As can be seen from Eqs [6 & 7], the phases of all participating wavefronts add up to give the phase of the image wave, that, in general, is given by:

$$\Phi i=\Phi c \pm (\Phi o-\Phi r) \qquad [11]$$

where i, c, o, and r are the indices of the image, reconstruction, object, and reference waves, respectively, and the sign "+" refers to the wave given by [6], and the sign "-" to the expression [7].

It is obvious that the product of two or more spherical phase factors, in general, is no longer spherical, i.e., deviations from the spherical shape occur (aberrations).

Expressions [6 & 7] must be of the form of [1.b], if the images are to be points with xi, yi, and zi being the coordinates of the image.

So, expression [6 & 7] and the image must have a similar spherical phase factor.

In this study, an attempt is made to fit [6 & 7] into the form of [1.b], doing a term-by-term matching of their respective series[9].

Matching of second-order phase terms in eqs [6 & 7] to the second-order phase term of eq. [1.b], yields a Gaussian focus at a distance from the origin given by

$$\frac{1}{Ri} = \frac{1}{Rc} \pm \frac{\mu}{m^2}\left(\frac{1}{Ro} - \frac{1}{Rr}\right) \qquad [12]$$

where $\mu=\lambda c/\lambda r$ and m is the enlargement of the hologram. The upper sign in eq.[12] is associated with expression [6] and the lower sign with expression [7].

Matching of the reminding second-order phase terms yields the direction of the Gaussian focus. The focus direction is given by the expressions

$$\frac{xi}{Ri} = \frac{xc}{Rc} \pm \frac{\mu}{m^2}\left(\frac{xo}{Ro} - \frac{xr}{Rr}\right) \qquad [13]$$

$$\frac{yi}{Ri} = \frac{yc}{Rc} \pm \frac{\mu}{m^2}\left(\frac{yo}{Ro} - \frac{yr}{Rr}\right) \qquad [14]$$

The wavefront aberration is defined as the phase difference between the desired spherical wave and the actual wavefront in the hologram plane.

The Seidel classical aberrations appears due to the mismatch between the third-and higher-order phase terms of eqs [6 & 7] and the third-order phase terms of the desired image wave.

The third-and-lowest-order phase errors $\Phi_3(x,y)$ (third-order aberrations) may be written in the form[13]

$$\Phi_3(x,y)= i\frac{2\pi}{\lambda c}\left\{-\frac{1}{8}\left[(x^2+y^2)^2S - 4(x^2+y^2)(xCx + yCy) +4(x^2Ax+ xyAxy+y^2Ay)\right]\right\} \qquad [15]$$

$$\Phi_3(x,y)= i\frac{2\pi}{\lambda c}\left\{\Delta S(x,y) + \Delta C(x,y) + \Delta A(x,y)\right\} \qquad [16]$$

where $\Delta(x,y)$ is the corresponding wavefront aberration, x, y are the hologram coordinates and S, Cx, Cy, Ax, Ay, Axy are the classical Seidel aberration coefficients.

The collection of the various terms yields phase-error terms associated with the various aberrations:

(a) Spherical aberration

$$S=\frac{1}{Rc^3}\pm\frac{\mu}{m^4}\left(\frac{1}{Ro^3}-\frac{1}{Rr^3}\right)-\frac{1}{Ri^3} \qquad [17]$$

(b) Coma

$$Cx=\frac{xc}{Rc^3}\pm\frac{\mu}{m^3}\left(\frac{xo}{Ro^3}-\frac{xr}{Rr^3}\right)-\frac{xi}{Ri^3} \qquad [18]$$

$$Cy=\frac{yc}{Rc^3}\pm\frac{\mu}{m^3}\left(\frac{yo}{Ro^3}-\frac{yr}{Rr^3}\right)-\frac{yi}{Ri^3} \qquad [19]$$

(c) Astigmatism

$$Ax=\frac{xc^2}{Rc^3}\pm\frac{\mu}{m^2}\left(\frac{xo^2}{Ro^3}-\frac{xr^2}{Rr^3}\right)-\frac{xi^2}{Ri^3} \qquad [20]$$

$$Ay=\frac{yc^2}{Rc^3}\pm\frac{\mu}{m^2}\left(\frac{yo^2}{Ro^3}-\frac{yr^2}{Rr^3}\right)-\frac{yi^2}{Ri^3} \qquad [21]$$

$$Axy=\frac{ycxc}{Rc^3}\pm\frac{\mu}{m^2}\left(\frac{yoxo}{Ro^3}-\frac{yrxr}{Rr^3}\right)-\frac{yixi}{Ri^3} \qquad [22]$$

Distortion and Field Curvature (they are astigmatic aberrations) do not appear in this formulation because these aberrations influence only the relative positions and forms of the various points in the object and image (they look like a kind of geometrical transformation)'[32]'. In this formulation, the object and image were considered to be points, so that relative position has no relevance.

In the xy plane the relevant aberration coefficients become, since yq=0 and Cy=Ay=Axy=0:

$$S=\frac{1}{Rc^3}\pm\frac{\mu}{m^4}\left(\frac{1}{Ro^3}-\frac{1}{Rr^3}\right)-\frac{1}{Ri^3} \qquad [17]$$

$$Cx=\frac{xc}{Rc^3}\pm\frac{\mu}{m^3}\left(\frac{xo}{Ro^3}-\frac{xr}{Rr^3}\right)-\frac{xi}{Ri^3} \qquad [18]$$

$$Ax=\frac{xc^2}{Rc^3}\pm\frac{\mu}{m^2}\left(\frac{xo^2}{Ro^3}-\frac{xr^2}{Rr^3}\right)-\frac{xi^2}{Ri^3} \qquad [20]$$

One of the problems with HOEs is to match the recording beam and the reconstruction beam. As the reconstruction beam is submitted to the application constraints, the only free parameters that we can control are with the recording beams.

The trouble may be avoided if we use aspherical wavefronts with certain characteristics as recording wavefronts. However, it is not always possible to generate the necessary aspherical wavefronts with COEs and, whenever possible, it is in general expensive.

Many methods have been proposed to obtain HOEs that present low aberrations[23,24,25,25,26,27, 28].

In this work, the recording wavefronts are derived from a CGH. Only the characteristics of these waves are needed, in order to obtain the numerical expression that will be used to generate these holograms. These recording wavefronts will permit to compensate the aberrations due to the mismatch.

The various objective is to obtain HOEs that present low aberrations. HOEs are to be recorded, each one exhibiting only one type of aberration (Coma, Astigmatism, Spherical Aberrations), when used in a certain geometry. We will try to elliminate these aberrations using aberrated wavefronts as recording wavefronts.

The coefficients of hologram aberration depend on the distances Rq and xq. Hence, if these quantities are properly chosen, the required aberration may be obtained from the reconstructed wavefront.

The desired amount of wavefront aberration is determined by the aberration at the edge of the hologram aperture.

The conditions for obtaining only Spherical Aberration (S) are A=0 and C=0. Then the condition $Rc=Ro=\infty$, $Rr=\mu Ri$, $xi=+xr$ and $\lambda c \neq \lambda r$ holds.

With these conditions the maximum spherical aberration at the edge of the aperture of diameter $2a$ is given by (eq. [12,17]),

$$\Delta s = \frac{1}{8Rr^3} a^4 (\mu^3 - \mu) \qquad [23]$$

For Coma, the condition is S=0 and A=0. One solution is Ro=Rr, $Rc=Ri=\infty$ and xo=-xr. Then the maximum coma is given, with $\lambda r=\lambda c$, by (eq. [12,13,18])

$$\Delta C = \frac{xo}{Ro^3} a^3 \qquad [24]$$

For Astigmatism, one has S=0 and C=0. A solution is Ro=Rr=Rc=Ri, xc=0, xr=-xo and xi=±2xr. For that condition the maximum Astigmatism is given, with λr=λc, by (eq. [12,13,20])

$$\Delta A = -\frac{xo^2}{2Ro^3}\alpha^2 \qquad [25]$$

Apendixe E1 shows a series of interferogram patterns corresponding to the various kinds of aberration[19].

# B1: CG Holography

1. Diffraction
2. 2-D Sampling Theorem
3. How to make a CGH

## Computer-Generated Holograms[33,34]

Holography, originally conceived as a new way of recording physical wavefronts, is now evolving to the point of recording nonphysical wavefronts. The key to this is the computer[35,36,37].

Optically formed holographic lenses (HLs) can be large, inexpensive, and lightweight. Unfortunately, they work well only illuminated by one of the incident wavefronts (angles, intensities, and wavelengths) used to record the hologram, and they present large aberrations due to the mismatch between the reconstruction wavefront and the reference wavefront. A computer optimization method allows us to design more flexible and general HLs and. CG Holography allows us to produce them[6,16].

Usually, it is not easy to record an aberrationless HOE with simple recording waves. One possible way to synthesize the desired recording waves is by means of computer-generated holograms (CGHs)[6,15]. These holograms can provide an arbitrary wavefront, and they have been exploited for various applications[33,34].

CGHs can also be applied to test optical systems, like aspheric surfaces[37], for image processing[38], for spatial filtering[35], for memories, three dimensional display purposes[39], etc..

Nowadays, different kinds of holograms can be generated by computer. This type of holograms have many useful properties. For example, an object does not have to exist; an ideal wavefront can be computed on the basis of the diffraction theory and be encoded into a tangible hologram.

In this work, we exploit CGHs for generating the recording aberrated waves, rather than as the final HOEs. These aberrated waves include terms such as the linear off-axis term (carrier) due to the necessity to separate the different diffraction orders from the zero-order.

As the knowledge of diffraction phenomena and the sampling theorem is essential to understand CG Holography, we will start with the discussion of these two subjects.

# 1. Diffraction

As the mechanism of holography reconstruction is based on light diffraction phenomena, we will make a short discussion of diffraction theory.

Light is a vectorial wave. However, for our propose, we shall assume the empirically established fact that holography phenomena may be accurately described by the approximation that light is a scalar monochromatic wave, which may be represented by a scalar function of the vector position $\vec{x}=(x,y,z)$ and time t.

The term diffraction has been defined by Sommerfeld as "any deviation of the light rays from rectilinear paths which cannot be interpreted as reflection or refraction".

The basic problem of diffraction is thus simply the determination of the manner in which a wave propagates from one surface to another, fig. 4.

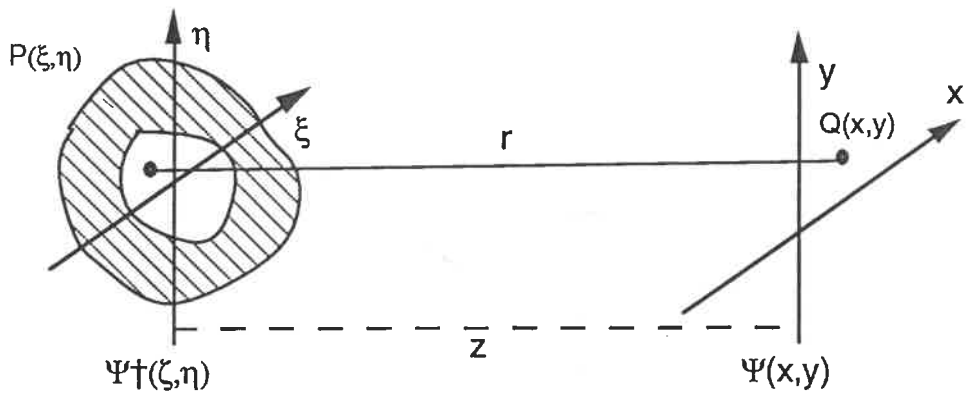


Fig. 4. Schematic diagram for diffraction analysis.

Thus, we shall be concerned with the solution of the scalar wave equation[2],

$$\nabla^2 E(\vec{x},t) = \frac{1}{c^2}\frac{\partial^2 E(\vec{x},t)}{\partial t^2} \qquad [26]$$

Where $E(\vec{x},t)$ is the optical disturbance, which, for monochromatic waves, takes the form $E(\vec{x},t) = \Psi(\vec{x})Exp(i2\pi\nu t)$, and c is the velocity of light.

Substituting the monochromatic form into the general wave equation, the time dependence is elliminated and the spatial part of the disturbance is seen to satisfy the Helmholtz equation:

$$\nabla^2\Psi(\vec{x}) + \left[\frac{2\pi\nu}{c}\right]^2\Psi(\vec{x}) = 0 \qquad [27]$$

One solution of this equation is the spherical wave, which is described by eq. [1.a].

If the disturbance across a planar aperture is described by a wave function $\Psi\dagger(\zeta,\eta)$ (here $(\zeta,\eta)$ is the position vector in the aperture plane), and accepting the point of view of the Huygens' principle which states that an arbitrary wave in any point in space (whose strength is given by the amplitude) simply a sum of spherical waves, then the field at point (x,y) beyond the screen is given by the expression (fig. 4)

$$\Psi(x,y) = \iint_A \Psi\dagger(\zeta,\eta)\,\Lambda(\zeta,\eta;x,y)\frac{e^{ik^*r(x,y;\zeta,\eta)}}{r(x,y;\zeta,\eta)}\,d\zeta d\eta \qquad [28]$$

where $\Lambda(x,h)$ is the inclination factor, which is related with the fact that the wave has a preferred direction, and r is the distance between points Q, in the (x,y) plane, and P, at the $(\zeta,\eta)$ plane.

Equation [28] is known as the Fresnel-Kirchhoff Integral diffraction.

We assume that $\Lambda(x,h)$ is essentially constant if we restrict (x,y) and $(\zeta,\eta)$ to suitably small regions in the neighborhood of the z axis.

The last expression shows that the function r occurs twice in the eq. [28], one in the denominator and another in the phasefuntion.

Because we restrict (x,y) and $(\zeta,\eta)$ as indicated above, we may regarde r as a slowly varying function in the denominator which affects only the amplitude of the wave; under this condition, r will not differ significantly from z.

However, r in the exponent affects the phase of the radiation, and is multiplied by $\frac{2\pi}{\lambda}$ (which is a very large number) and cannot be replaced simply by z (for the resulting errors will be multiplied by this large number and, consequently, can generate phase errors much greater than $2\pi$ radians).

Further simplification can be accomplished only by adopting certain approximations to the quantity r in the exponent of eq. [28].

We may write r as:

$$r(x,y;\zeta,\eta)=\sqrt{(x-\zeta)^2+(y-\eta)^2+z^2}$$

or

$$r=R\sqrt{1+\frac{\xi^2+\eta^2}{R^2}-2\frac{\xi x+\eta y}{R2}} \qquad [29]$$

where $R=\sqrt{x^2+y^2+z^2}$.

If we restrict our attention to relatively large distances, so that eq. [29] may be expanded in a binomial series and approximated by its first three terms, i.e., the square root in eq. [29] is adequately approximated by the first three terms of its expansion. We have, thus

$$r= R - \frac{\xi x+\eta y}{R}+\frac{\xi^2+\eta^2}{2R} \qquad [30]$$

This assumption allows the $\Psi$ function to be written as:

$$\Psi(x,y) = \frac{C}{z} e^{ikR} \int_{-\infty}^{+\infty} \int_{-\infty}^{+\infty} \Psi^{\dagger}(\zeta,\eta) e^{ik\left(\frac{\xi 2+\eta 2}{2R} - \frac{\xi x+\eta y}{R}\right)} \, d\zeta d\eta \qquad [31]$$

When the distance z is sufficiently large for this approximation to be accurate, the observer is said to be in the region of Fresnel diffraction.

If the distance is sufficiently large, so that $k\left(\frac{\xi^2+\eta^2}{2R}\right) << 1$, meaning that we now restrict our attention to relatively large distances, eq. [30] may be approximated by its first two lower order terms. This condition is called the "far-field" approximation, and the region where it is valid is the region of Fraunhofer diffraction.

Using the last condition, and noting that $z^2 >> x^2+y^2$, we obtain for the field

$$\Psi(x,y) = \frac{C}{z} e^{+ikz} \int_{-\infty}^{+\infty} \int_{-\infty}^{+\infty} \Psi'(\zeta,\eta) e^{-i\frac{k}{z}(\xi x+\eta y)} \, d\zeta d\eta \qquad [32]$$

The analysis of the last expression shows that the observed field distribution can be found directly from the Fourier Transform (FT) of the aperture distribution itself, evaluated at frequencies $\left(fx=\frac{\xi}{\lambda z}\right.$, $\left. fy=\frac{\eta}{\lambda z}\right)$.

In many practical situations the approximation $k\left(\frac{\xi^2+\eta^2}{2R}\right) << 1$ is not possible; however, the term $\frac{\xi^2+\eta^2}{2R}$ can be elliminated if we place a lens in the plane $(\zeta,\eta)$ and observe the diffraction pattern formed at the focus of the lens, thus elliminating that term.

We can define a lens as a device that converts a plane wave into a spherical wavefront of radius f. The concept is illustred in fig. 5.

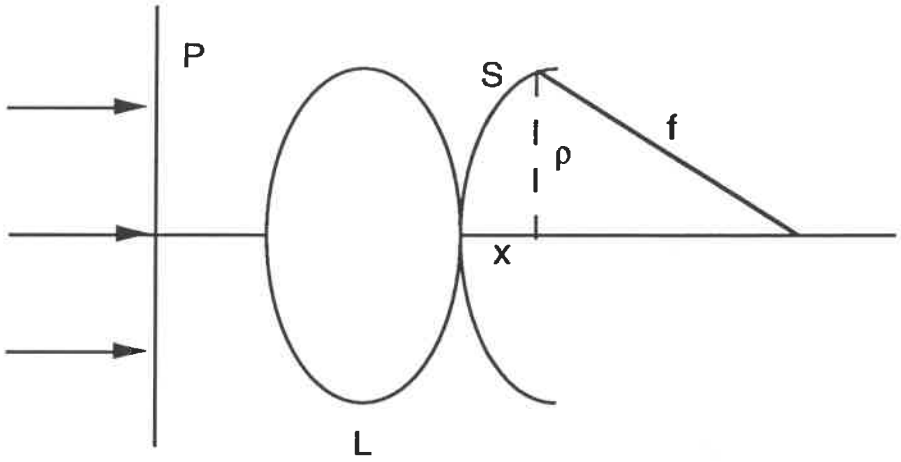


Fig. 5. Schematic diagram for lens analysis, demonstrating the conversion of a plane wavefont to a spherical wavefront of radius f.

In figure 5, P is a plane wave incident on the lens L; S is a spherical wave emergent from the lens; ρ is the radial height to an arbitrary point on S; and x is the radial distance from the foot of the perpendicular from S to the wavefront.

From the Pythagorean theorem, we have $(f-x)^2+\rho^2=f^2$ or $2fx=\rho^2-x^2$. For paraxial optics, x is small and hence $x^2$ may be ignored by comparison. Thus $x=\frac{\rho^2}{2f}$. This equation is referred to as the "sagital" approximation. The phase change introduced by a lens is therefore $\phi=kx=k\frac{\xi^2+\eta^2}{2f}$. The lens placed in the $(\zeta,\eta)$ plane yields an additional term $\mathrm{Exp}[-ik\frac{\xi 2+\eta 2}{2f}]$ because it produces a converging spherical wave.

This term cancels the term in $(\xi^2+\eta^2)$ arising from eq. [31] when z=f. Thus, the field at point (x,y) in the focal plane is given by

$$\Psi(x,y)=\frac{C}{f}e^{+ikf}\int_{-\infty}^{+\infty}\int_{-\infty}^{+\infty}\Psi'(\zeta,\eta)e^{-i\frac{k}{z}(\xi x+\eta y)}\,d\zeta d\eta \qquad [33]$$

Note that eq. [33] is identical to eq. [32] if f is substituted for z. These equations state that the field in the far zone or in the focal plane of the lens is the FT of the field across the diffracting aperture.

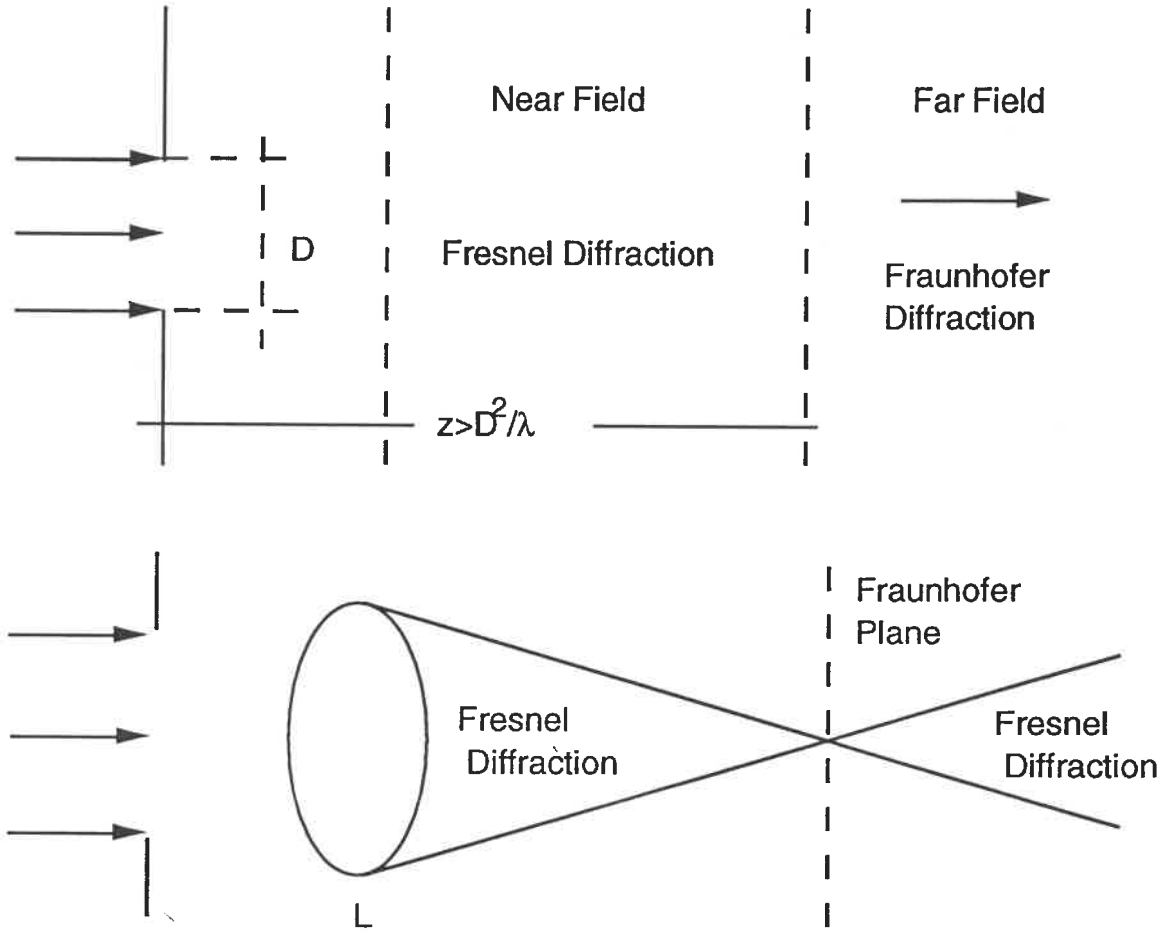


Fig. 6. Schematic layout illustrating the differences between Fraunhofer and Fresnel diffraction from the aperture with and without a lens.

Note that in the region nearest to the aperture these approximations are not valid, and the complete expression must be used (eq. [28]).

## 2. Two-Dimensional Sampling Theorem[30,31,41]

In Computer-Generated Holography (CG Holography), given the desired image and the reconstruction beam, the amplitude transmittance of a hologram is calculated by a computer.

As a computer can only describe a function by its values taken at a discrete set of points, rather than attempting to describe it everywhere in a continuous fashion, the calculated pattern must satisfy the sampling theorems and must not exceed the resolution capability of the recording device.

Therefore, the hologram transmittance H(x,y) will be represented by a set of sampled values (the values of the function obtained at the sampling points). One must be careful to satisfy the classical sampling theorems of Shannon, Whittaker, Kotelnikov, and Nyquist.

The separation of the sampling points is called the sampling interval, and the inverse of the sampling interval is called the sampling rate (or sampling frequency).

The sampling theorem basically states that any band-limited function can be specified exactly by its sampled values, taken at regular intervals, provided that these intervals do not exceed some critical sampling interval.

When we say that the function is band-limited we mean a function with Fourier transform that is nonzero over only a finite region $\mathfrak{R}$ of the frequency space. See, in figure 7, an example for a one-dimensional function f(x).

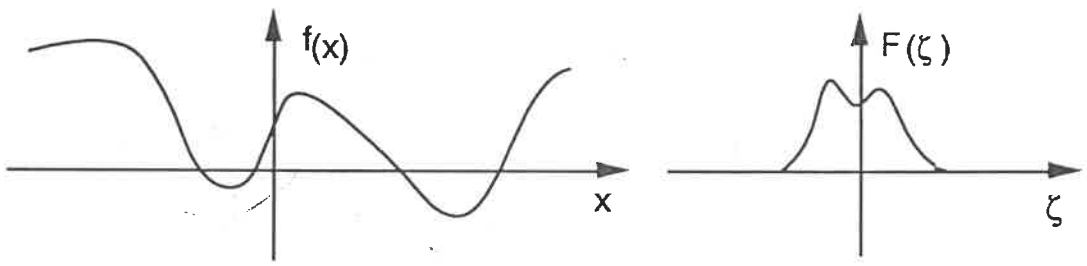


Fig. 7. A band-limited function f(x) and its spectrum F(ζ).

In spite of the fact that a computer only works with sets of sampled values, we can exactly reconstruct a sampling signal if the original signal was sampled in accordance with the sampling theorem.

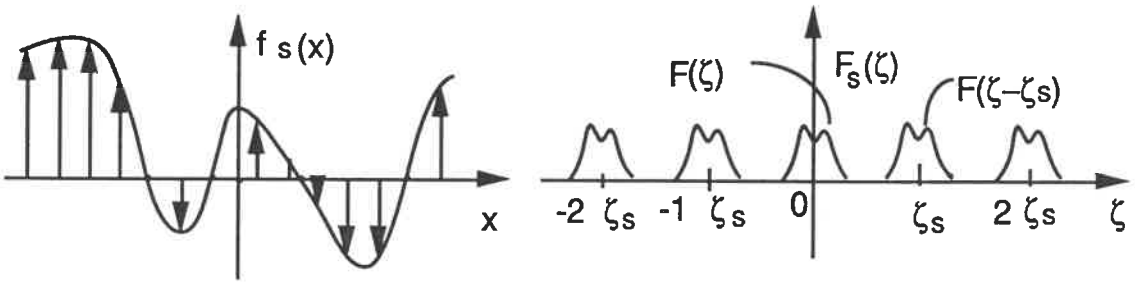


Fig. 8. Sampled version $f_s(x)$ of f(x) and its spectrum $F_S(\zeta)$.

As shown in fig. 8 the spectrum of the sampled function is composed by a set of copies of the spectrum of the nonsampled function, repeated at sampling intervals. So, if we pass $f_s(x)$ through a low-pass filter, f(x) can be recovered from $f_s(x)$.

As the hologram transmittance is a two-dimensional function, we will make the analysis of the two-dimensional sampling theorem. So, if a two-dimensional function H(x,y) contains no frequencies higher than B line/mm (the function is bandlimited), this function is completely determined by giving its values at a set of points extending throughout the space domain and spaced at less or equal than 1/2B.

So, in our case, we will replace the function H(x,y) by an array of its sampled values taken at a discrete set of points in the xy plane.

Considering a rectangular lattice of samples of function H(x,y), as defined by[30]

$$Hs(x,y)=comb(\tfrac{x}{X}).comb(\tfrac{y}{Y}).H(x,y) \qquad [34]$$

where $comb(\frac{x-x_o}{b})=|b|\sum_{n=-\infty}^{\infty}\delta(x-x_o-nb)$

The sampled function Hs thus consists of an array of Dirac δ functions, spaced at intervals of widths X in the x direction and Y in the y direction. The area under each δ function is proportional to the value of the function H at that particular point in the rectangular sampling lattice.

It is possible to show that the spectrum of the sampled function is given by[30]

$$\tilde{H}s(fx,fy)=\sum_{n=-\infty}^{\infty}\sum_{m=-\infty}^{\infty}\tilde{H}(fx-\frac{n}{X},\ fy-\frac{m}{Y}) \quad [35]$$

Thus $\tilde{H}s$ is seen to consist of a set of functions each having the form of $\tilde{H}$ repeated at intervals 1/X, 1/Y along the frequency axes fx and fy, respectively. The various replicas of $\tilde{H}$ are often referred to as the spectral orders of $\tilde{H}s$ , with $H(fx-\frac{n}{X},\ fx-\frac{m}{Y})$ known as the nth spectral order.

In accordance with what we have assumed about the function H, its spectrum $\tilde{H}$ is nonzero over only a finite region $\mathfrak{R}$ of the frequency space. This means that the spatial frequency spectrum is essentially zero outside the bandwidth, i.e., fx, fy $\leq \Delta f/2$ where $\Delta f$ is the largest dimension of region $\mathfrak{R}$.

As implied by Eq. [35], the region over which the spectrum of the sampled function is nonzero can be found by constructing the region $\mathfrak{R}$ about each point (n/X,m/Y) in the frequency plane.

It becomes clear that if X and Y are sufficiently small(i.e., the samples are sufficiently close together), then the separations (1/X,1/Y) of the various spectral orders will be large enough to assure that adjacent orders do not overlap.

In order to determine the maximum allowable sparation between different orders in the frequency plane, let 2Bx and 2By represent the widths in the fx and fy directions (the highest signal frequencies), respectively, of the smallest rectangle that completely encloses the region $\mathfrak{R}$.

Since the various terms in the spectrum eq. [35] of the sampled data are separated by distances 1/X and 1/Y in the fx and fy directions, respectively, separation of the various spectral orders is assured if

$$X \leq \frac{1}{2Bx} \quad \text{and} \quad Y \leq \frac{1}{2By} \qquad [36]$$

Let us briefly review the above development. If H(x,y) is band-limited, such that $\tilde{H}(fx,fy)=0$ for $|fx|>Bx$ and $|fy| >By$, and if the sampling is used to obtain Hs(x,y), then H(x,y) can be recovered from Hs as long as the sampling rates 1/X, 1/Y are at least as great as the total spectral widths 2Bx and 2By, respectively.

Thus, the critical sampling rates are just 1/X and 1/Y, for each axis, and the critical sampling intervals are X and Y for the fx and fy axis, respectively. We shall also refer to these quantities as the Nyquist rate and Nyquist interval, respectively.

## 3. How to make a CGH[33,34,40]

When you make an ordinary hologram (OH) we photograph a standing wave pattern or interference pattern formed when mutually coherent object and reference wavefronts meet at the photographic recording medium. The object wavefront, represented by the electric vector O(x,y), and the reference wavefront, R(x,y), form an interference pattern of irradiance I(x,y) (eq. [3]) in the recording plane (the x-y plane).

The mechanism of holography reconstruction is based on diffraction of the reconstruction beam. So, a hologram can be seen as a "distorted" diffraction grating[30,31].

So, if you could make a distorted diffraction grating with an amplitude transmission H(x,y)=I(x,y) and illuminate it by the reconstruction beam C, we would form the three common wavefronts in holography. Given C and R it is only necessary to calculated O for obtain H.

The calculated pattern must not exceed the resolution capability of the recording device. Presuming these precautions are observed, the only real problem is calculating O. But that is sometimes, a very big problem.

A true CGH may be difficult to calculate and difficult to write. First, optical holograms often form images with $10^5$ to $10^8$ picture elements in each direction, yet $10^4$ pixels can present a problem to the computer. Also, representing a 3D object as a collection of $10^6$ or (hopefully) more points is very difficult.

An overall scheme for CG Holography is shown in fig. 9. It includes the following entities and processes[37]:

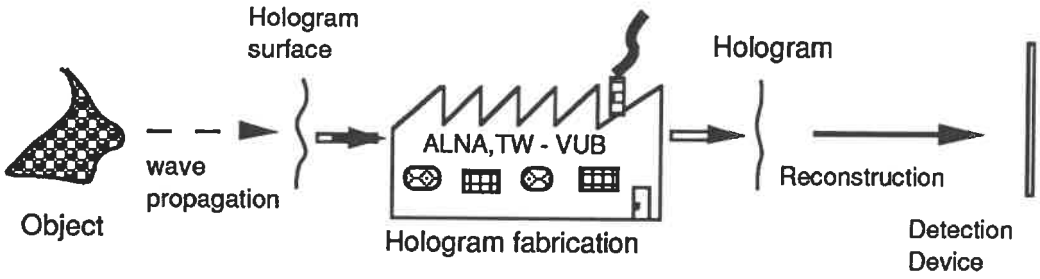


Fig. 9. Scheme for CG holography at ALNA-TW, VUB

*Object* The object needs not to exist physically; it can be imaginary or idealized, it can radiate or be illuminated by an external source.

*Wave propagation* Wave propagation is computed with the theories appropriate for Fraunhofer, Fresnel, or near-field diffraction.

*Hologram surface* The object scattered field is evaluated on a hypothetical surface, which is usually flat.

*Hologram fabrication* The irradiance on the hologram surface is represented by a transparency produced by a computer driven plotter, laser beam, or electron beam on correspondingly diverse materials. The hologram writing requirements vary widely with the application. Scale reduction is usually necessary for reconstruction with visible light or other radiation of similar wavelength.

*Hologram* The computer generated hologram is a tangible mask with spatially variable transmittance.

*Reconstruction* The hologram is illuminated, and the diffracted wave propagates towards a detection device.

The realization of a digital hologram is done, basically, in three steps: the design step, the computation step, and the implementation step[34].

In the design step one must solve the design problems, but also think of additional quality constraints, diffraction efficiency, signal-noise ratio (SNR), wavefont accuracy and cost. The method chosen to compute the hologram, the algorithm, the encoding and realization problems depend on this step.

The computation step is software-oriented. It is a translation of the design considerations toward the generation of the CGH-data and the encoding phase process.

The last step is the fabrication of the CGH. This is the major problem in synthetic holography, a technological problem: how to implement efficiently NxM encoded complex samples into a physical hologram.

First step

When we are reading a hologram we have the reconstruction wave A(x,y), the holographic plate H(x,y), and the image wave $I(\zeta,\eta)$. The mechanism of reconstruction is based on the diffraction of the readout beam. So, a hologram can be seen as a distorted diffraction grating.

The computation of a CGH is not restricted to the calculation or simulation of the fringes obtained by the interference of the reference wave and the object wave. This would be complicated in most cases, due to the nonexistence of the object wave (in other words, a second wave source).

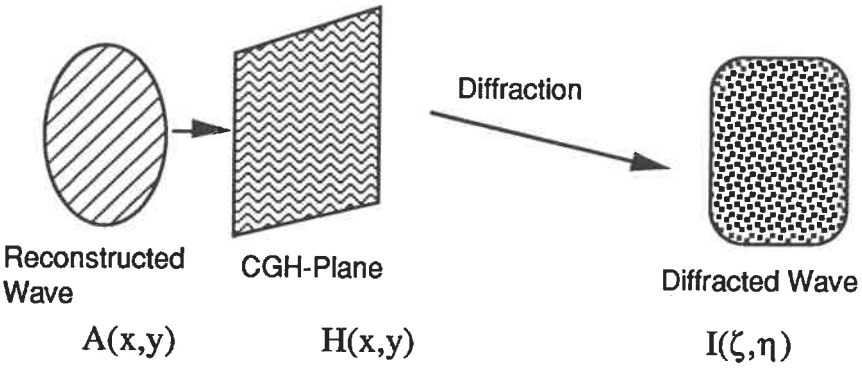


Fig. 10. CGH realization: generate a diffraction grating H(x,y) that diffracts a given wave A(x,y) into a desired diffracted wave $I(\zeta,\eta)$.

So, the question is: what kind of diffraction grating H(x,y) illuminated by a given wavefront A(x,y) generates the wanted $I(\zeta,\eta)$? The wanted $I(\zeta,\eta)$ is the desired diffracted wave (image) with high diffraction efficiency, high SNR, high wavefront accuracy and produced at low cost.

We know that $I(\zeta,\eta)$ is a free space transformation of the product H(x,y).A(x,y), see fig.10, given by a general diffraction operator Fresnel-Kirchhoff Integral[30,31,41] (eq. [28]).

$$I(\zeta,\eta) = K\iint H(x,y)A(x,y)\frac{e^{ikr(x,y;\zeta,\eta)}}{r(x,y;\zeta,\eta)}d\zeta d\eta \qquad [37]$$

If the inversion of this operator is possible we obtain

$$H(x,y) = D_{(\zeta,\eta;x,y)}\left\{\frac{I(\zeta,\eta)}{A(x,y)}\right\} \qquad [38]$$

since A(x,y) is known. $D_{(\zeta,\eta;x,y)}$ represents the inverted diffraction operator "Fresnel-Kirchhoff Integral". But now we may have another problem: is this inversion mathematically consistent, i.e., does $D_{(\zeta,\eta;x,y)}$ always exit?

In many practical cases the diffraction operator reduces to a Fourier transform of the product H(x,y).A(x,y). In these cases the inverted diffraction operator exists, it is the inverse FT.

However, the realization of CGHs is very similar for the different diffraction regimes.

H(x,y) is the diffraction pattern which we need.

Second step

The computation problem of the CGH is defined when a reconstruction beam (2D light distribution), a diffracted beam , a wavelength, and the distance between the CGH and the diffraction plane are given.

One must first determine the size, spatial frequency and resolution of the CGH which are consistent with the available equipment.

Most of the calculations of CGHs use the 2D Fourier Transform (FT), which is easily implemented using a FFT (Fast FT) algorithm. This model of the CGH computation is sufficient, in the sense that, in general, one needs only the 2D spatial distribution. It is not necessary to take into account the absolute amplitude and the phase variations in the direction perpendicular to the diffracted plane.

The CGH will consist of MxN samples, M and N being the number of samples taken in each direction. The number of samples depends on the image size and the image resolution. The number MxN is called the space bandwidth product (SBWP), SBWP=MxN.

The transmittance of the CGHs used in this work has the form of the function $t(x,y) \alpha I(x,y)$ given in eq. [3]. Because the function t(x,y) is already real and nonnegative, the computer simply calculates its values at discrete intervals, encodes this sampled function and produces a graphical output of the final pattern on a printer or other device.

The sampling rate for the function t(x,y) is proportional to the total bandwidth of the function.

We assume that image width and height are, respectively $\Delta x$ and $\Delta y$. If $\delta_x$ and $\delta_y$ are the resolution element size in the image, the number of resolvable points in the object (the function to be implemented in CGH) is

$$NxM=\frac{\Delta x}{\delta_x}\frac{\Delta y}{\delta_y} \qquad [39.a]$$

For our objects we will take M=N, then making $\delta_x=\delta_y$ and $\Delta x=\Delta y$, with $\delta_x=(\Delta f)^{-1}$ , where $\Delta f$ is the bandwidth of the object

$$N^2=\frac{\Delta x\Delta y}{\delta_x{}^2}=(\Delta x)^2(\Delta f)^2 \qquad [39.b]$$

The hologram is assumed to have at least $N^2$ points to preserve the information, thus

$$(\frac{\Delta f}{\delta_v})^2 \geq (\frac{\Delta x}{\delta_x})^2=(\Delta x\Delta f)^2 \qquad [40]$$

In fact, $\delta_v$ was taken to be $\Delta x^{-1}$ on basis of the sampling theorem.

Encoding[40]

In this phase we have the wavefront of the object defined as a complex function.

Once the hologram transmittance is calculated analytically or based on 2D FFT, the CGH encoding can start. In general the encoding process will permit us to transform the complex values of the CGH computation into a physical representation.

The phase function that we want implement in the desired CGH is

$$H(x,y)=\varphi c(x,y)+\Phi 3(x,y) \qquad [41]$$

The amplitude transmittance of the CGH is made to have the form

$$t(x,y)=b+a(x,y)\cos H(x,y) \qquad [42]$$

like in a ordinary hologram, where $b \leq 0.5$ is the bias, and $a(x,y) \leq 0.5$ is the modulation.

The encoding method that was used in our CGHs is the Lee method[42].

We may present this encoding method in the following form[33,38]:

$$t_B(x,y)=1 \quad \text{if} \quad [1+\cos H(x,y)] \geq 1$$
$$t_B(x,y)=0 \quad \text{if} \quad [1+\cos H(x,y)] < 1 \qquad [43] \quad .$$

where t(x,y) represents the CGH transmittance.

This method permits encoding of a phasefunction in the form of binary-transmittance values.

The CGH obtained with this technique belongs to the class of Binary-Phase CGH.

Third Step

Now we have the hologram computed. It is necessary to fabricate it physically.

Many different techniques are possible[34]. The technique that presents better performance based in microlithography, as electron beam plotting. This technique offers resolutions lower than 1 μm, but is expensive. Therefore, it is not easy to find this equipment in many laboratories.

A more accessible method is photoreduction: the CGH is printed macroscopically using a good printer (usually a laser printer), and afterwards this macroscopic mask is reduced, using a photoreduction device into a high resolution photographic plate.

## B2: Realization of a CGH

1. Design Constraints

2. Experimental Parameters and Fabrication of CGHs

## 1. CGH Design Constraints

In order to alleviate aberrations in a HOE, it would be useful to compensate the aberrations by recording the HOEs with an aberrated wavefront. Such an aberrated wavefront can be described by a polynomial expansion in Cartesian coordinates[32],

$$H(x,y;\lambda c)= \frac{2\pi}{\lambda c} \sum_{m,n} a_{mn}\, x^m y^n \quad [44]$$

This wavefront can be realized with a CGH as in fig. 11.

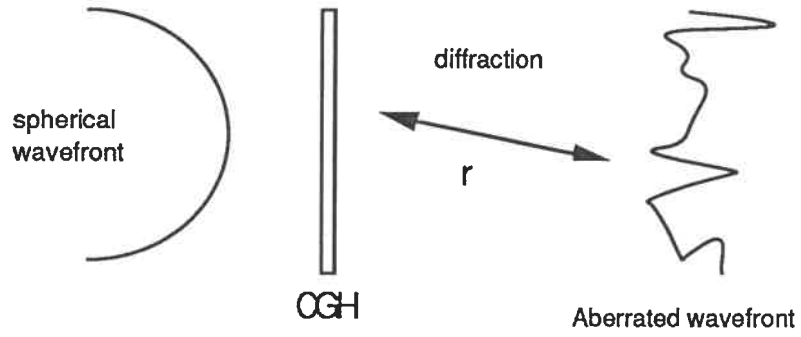


Fig. 11. Wavefront aberration with a CGH[14]

The CGH must have the capacity to transform a spherical phase distribution into a distribution given by eq. [44].

The aspheric wavefront generated by a CGH is afterwards used for optical recording of the HOE. For each type of aberration we will record HOEs both with aberrated wavefronts and without, in order to compare results.

We look now for the experimental conditions under which the overall holographic process produces the desired wavefront aberrations.

Uncorrected HOEs were recorded with a similar set-up as the corrected HOE, but in this case the CGH used only contain a linear phase.

From equations [15, 16 and 17], we find that the coefficient of hologram aberrations depends on distances Rq and xq.
Hence, if these quantities are properly chosen, the required aberrations may be obtained from the reconstructed wavefront.

The wavefront phase in the CGH will be the sum of the third-order phase errors wavefront $\Phi_3(x,y)$ and the carrier wavefront phase $\varphi_c(x,y;\lambda c)$, i.e., the phase function of the CGH should be[18]

$$T(x,y)=\Phi_3(x,y;\lambda c) + \varphi_c(x,y;\lambda c) \quad [45]$$

where $\varphi_c(x,y;\lambda c)=\frac{2\pi}{\lambda c}$ x.sinθ, is the carrier for off-axis reconstruction.

Considering the continuous CGH transmittance,

$$T(x,y)=\Phi_3(x,y;\lambda c) + \varphi_c(x,y;\lambda c) \quad [46]$$

It should fulfill the sampling criterion. The highest sampling frequency is the CGH resolution fs, thus

a) $$\sqrt{\left[\frac{\delta T(x,y)}{\delta x}\right]^2 + \left[\frac{\delta T(x,y)}{\delta y}\right]^2}\Bigg|_{max} < \pi\, fs \quad [47]$$

To avoid the overlap of diffraction orders, the third-order phase errors wavefront $\Phi_3(x,y)$ must satisfy the following condition:

b) $$\frac{\delta \Phi 3(x,y)}{\delta x}\Bigg|_{max} < \frac{2\pi}{\lambda c} x\ \sin\theta \quad [48]$$

The smallest aberration that can be realized is given by:

c) $$\sqrt{\left[\frac{\delta \Phi_3(x,y)}{\delta x}\right]^2 + \left[\frac{\delta \Phi_3(x,y)}{\delta y}\right]^2}\Bigg|_{min} > \frac{\lambda c}{2a} \quad [49]$$

where a is the aperture radius.

So, we have to satisfy the following conditions:

$$\text{i)} \quad \frac{\lambda c}{2a^4} < S < fs\,\frac{\lambda c}{2\sqrt{3}a^3} \qquad [50]$$

$$\text{ii)} \quad \frac{\lambda c}{2\sqrt{6}a^3} < C < fs\,\frac{\lambda c}{2\sqrt{10}\,a^2} \qquad [51]$$

$$\text{ii)} \quad \frac{\lambda c}{2a^2} < A < fs\,\frac{\lambda c}{4\sqrt{2}a^2} \qquad [52]$$

We see that conditions a),b) and c) can be used to check the feasibility of realizing a given aberrated wavefront with a CGH.

We will take $\Delta S \approx 10\lambda$, $\Delta C \approx 11\lambda$ and $\Delta A \approx 50\lambda$ (eq. [23, 24, 25]), to assure that the aberrations of the wavefront coming from the CGH are larger than the other possible existing aberrations introduced by lenses, mirrors and beamsplitter. These were estimated to be of the order of $\lambda$. $\Delta S$, $\Delta C$, $\Delta A$ are of the order of $10\lambda$.

In this work we tried to include in the CGH the complete reference wave (aberrated spherical wave) that would be used to make the HOEs. However, this could not be realized because the SBWP of the complete wavefront is larger than the SBWP of our printer.

## 2. Experimental Parameters and Fabrication Constraints

If we take fs= $\frac{2048}{2a}$ (fs=$\frac{N}{2a}$ the highest sampling frequency), the experimental parameters which produce the desired wavefront aberrations are:

for spherical aberration

zr=5 cm and xr=1 cm;

for coma and astigmatism

zr=20 cm and xr=5 cm.

Rewriting the phase of the wavefront aberrations in the polynomial form

$$\Phi(x,y;\lambda c)=\frac{2\pi}{\lambda c}\sum_{m,n} a_{mn}\, x^m y^n \qquad [53]$$

and calculating the $a_{mn}$ coefficients in order to know the CGH transmittances, we only need to introduce the CGH-Data in the computer for each CGH mask.

The CGHs presented here are computed with SR53 software developed by Steve Roose, on a Apple Macintosh IIx computer, having a RAM of 4 Mbytes, an 80 Mbytes harddisk, and a mathematical coprocessor MC68881.

The patterns obtained are shown in the next four pages.

The patterns were drawn onto a transparency using a Laser printer (LaserWriter Plus) with a resolution R=118 dots/cm and an aperture A=18 cm (the maximum size of A4 format that can be used for drawing is 18x18 $cm^2$) and thus N=RxA=2100, resulting in a SBWP≈$4x10^6$ points.

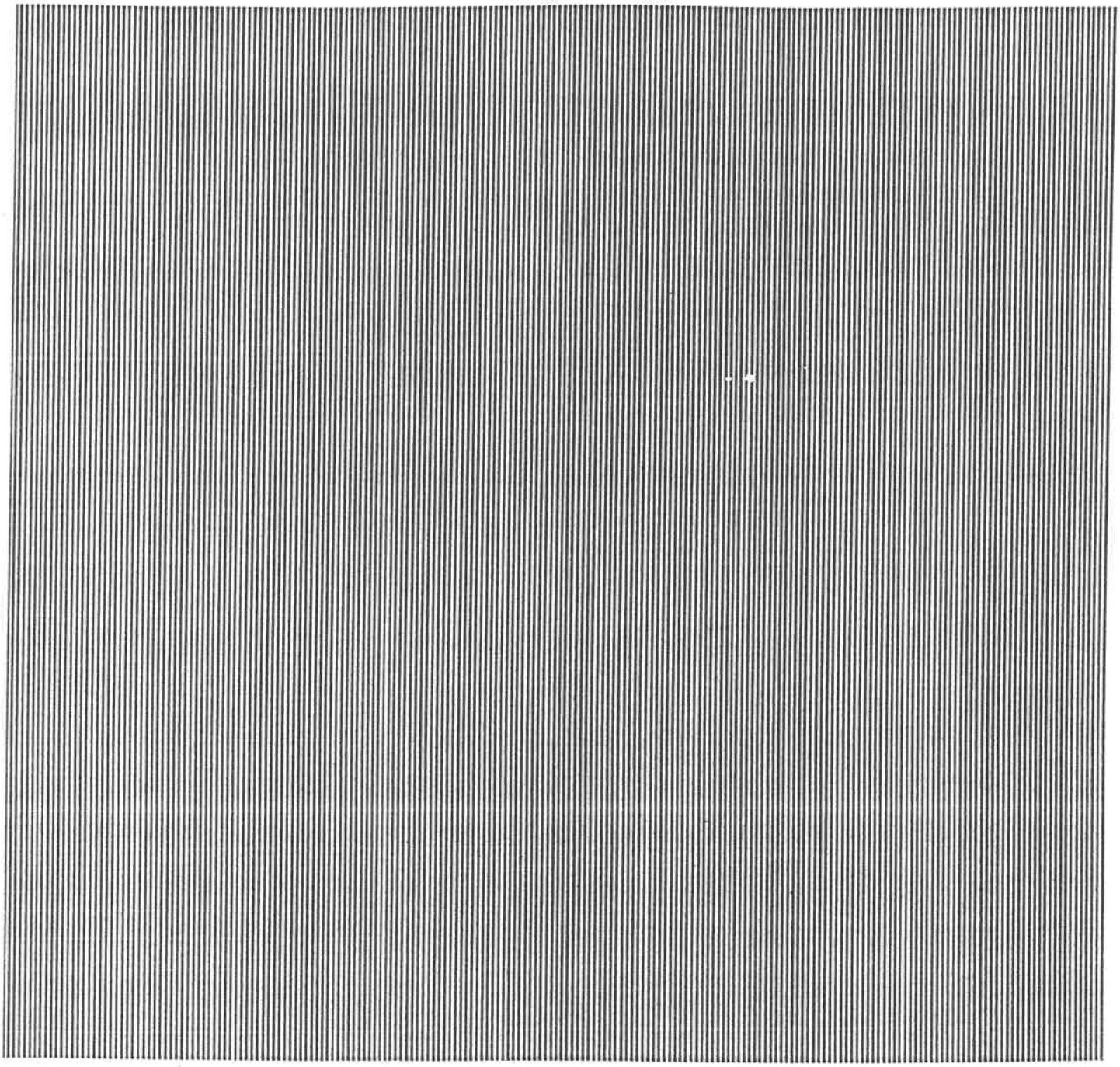

Carrier

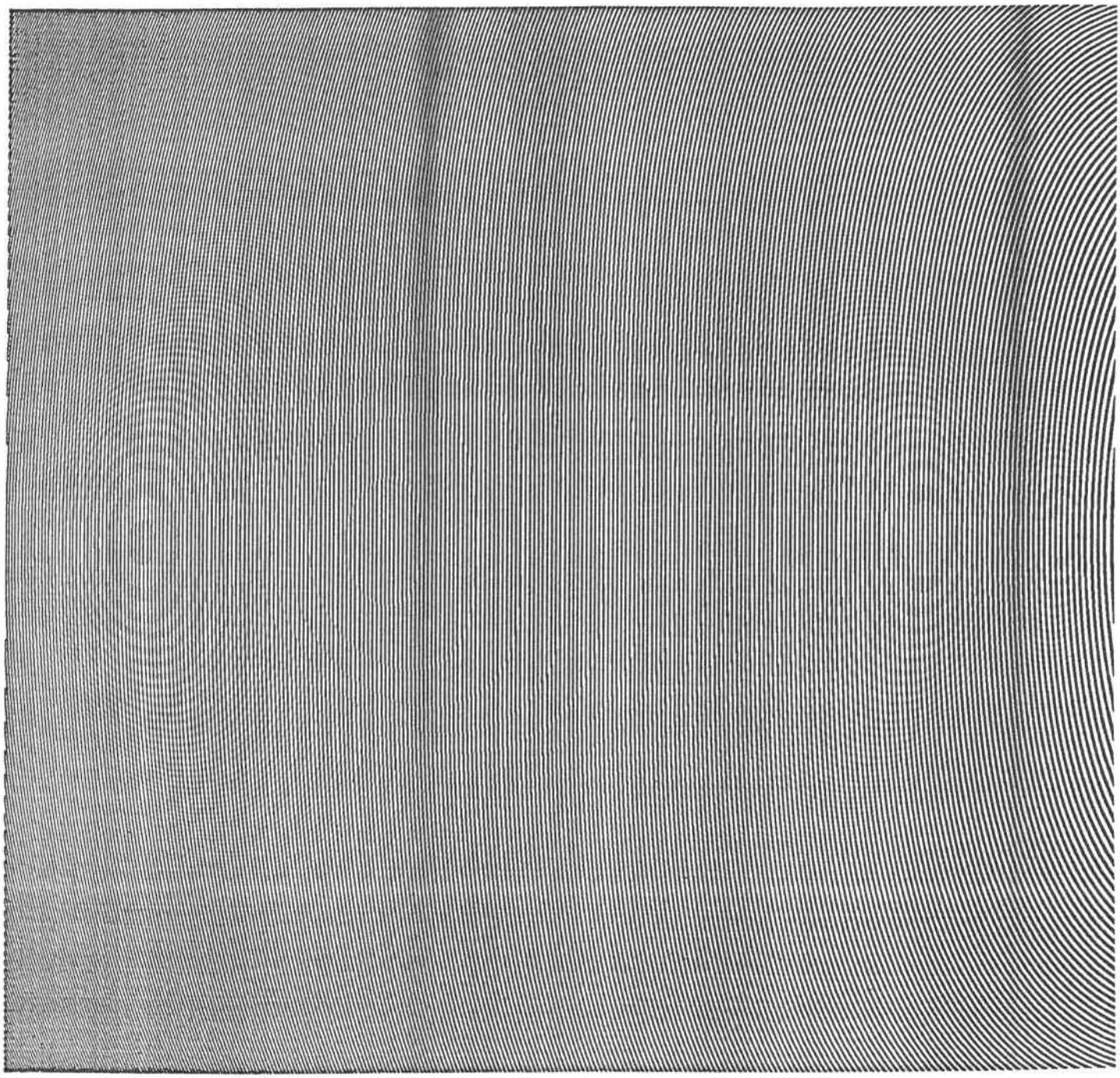

Spherical Ab. + Carrier

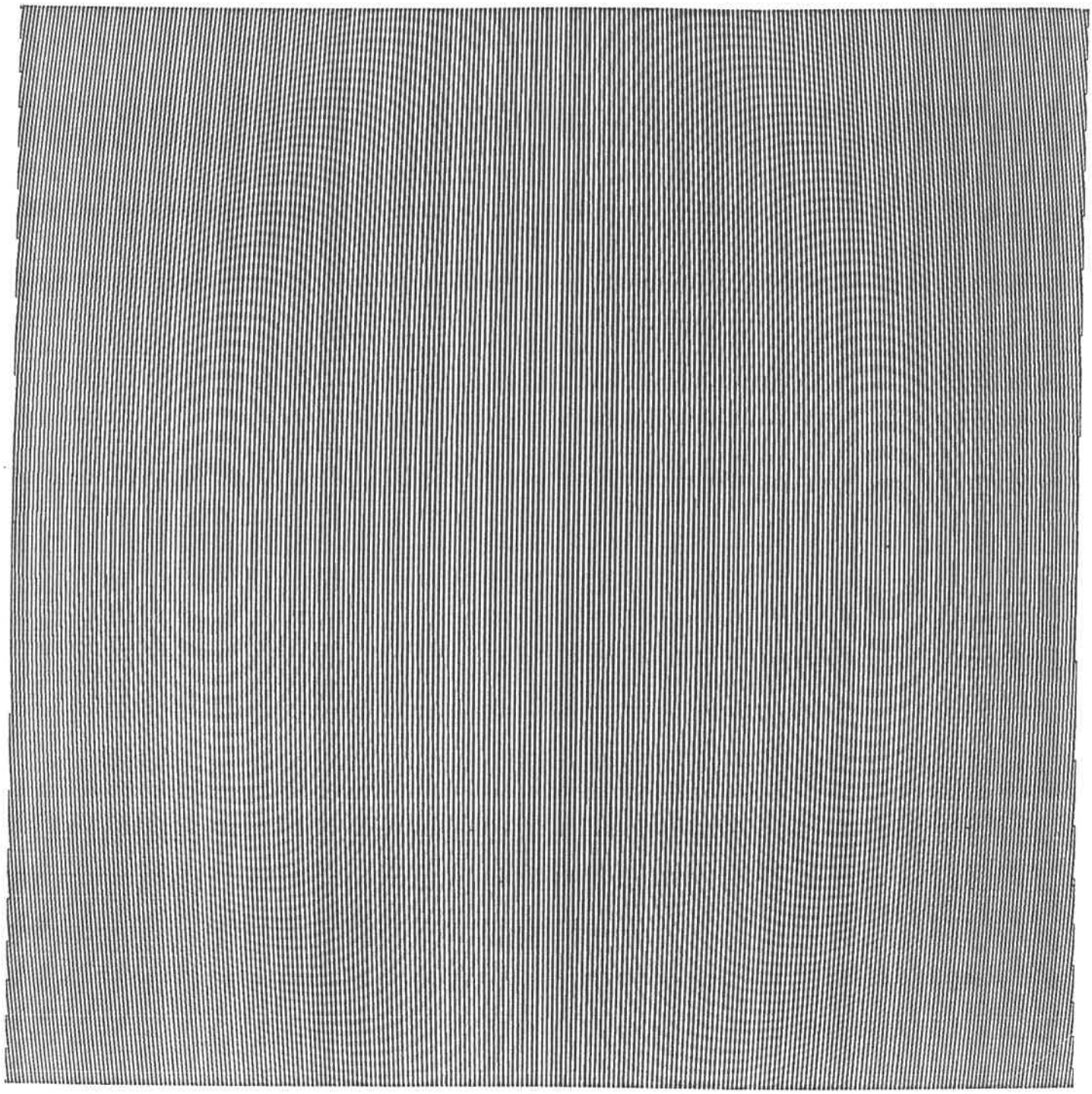

Coma + Carrier

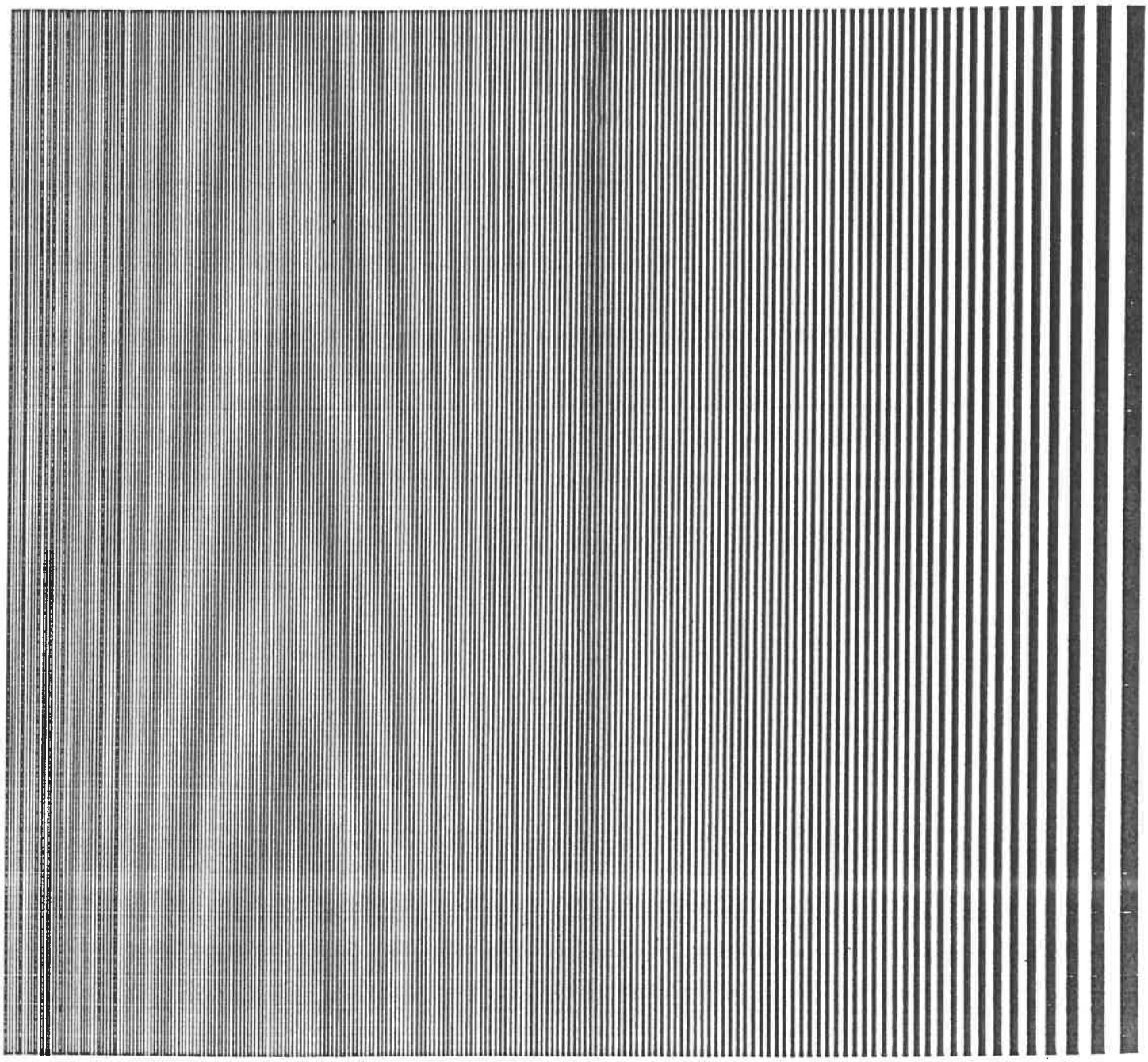

Astigmatism + Carrier

It is the resolution of the printer and the page size which limit the SBWP of the CGH.

After this, we made the necessary reduction of the interferogram. The size of each interferogram was reduced 18 times, using a photoreductor existent at VUB, fig. 12.

The photoreduction set up uses a simple lens with focal distance of 10 cm and diameter of 10 cm. The response limit to spatial frequencies is estimated experimentally at 200points/mm[38].

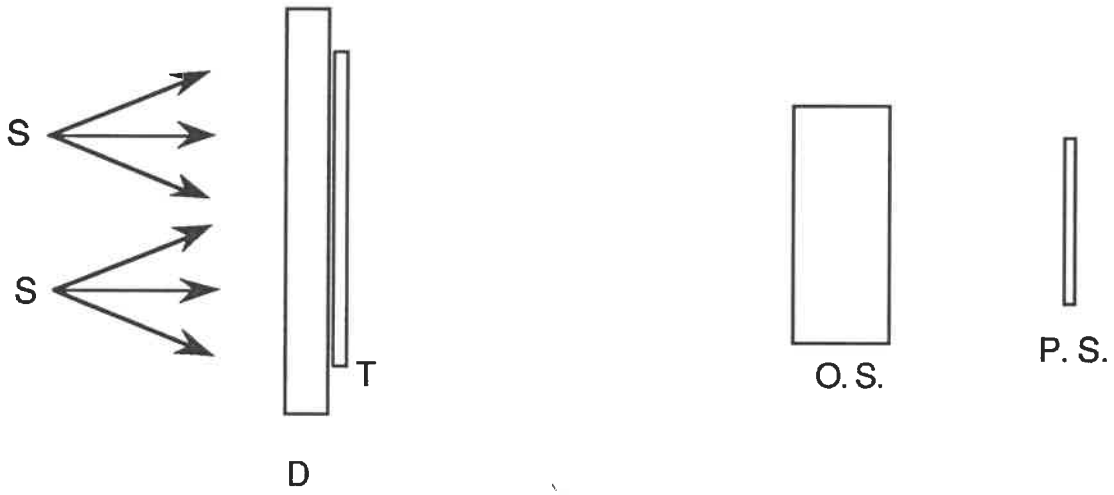


Fig.12. Scheme of the VUB photoreductor principle, where S is an incoherent source (halogen lamp, 1000 W), D is the diffusor screen, T is the transparency, S.O. is the optical system (photographic objective) and P.S. is film support, positionned at the image plan.

The plates used for the mask were Millimask Plates HD Agfa Gevaert. These plates have high resolution, 2000 lin/mm. The size of the final hologram is 10 mm X 10 mm.

The reconstruction of the CGH is similar to that of optical holograms (OH).

In appendix E2, we describe all phases of the development, and the solutions used.

# Part II: Fabrication and Testing of HOEs and CGHs

C1: Set-up for test of CGHs

C2: Set-up used to record HOEs

C3: Set-up used to analyze HOEs

# C1: Set-up for Test of CGHs

In order to test the fidelity of the wavefronts produced by CGHs, their reconstructions were interfered with a plane wave, using the arrangement shown in fig. 13 (Mach-Zehnder Interferometer[43] (MZI)).

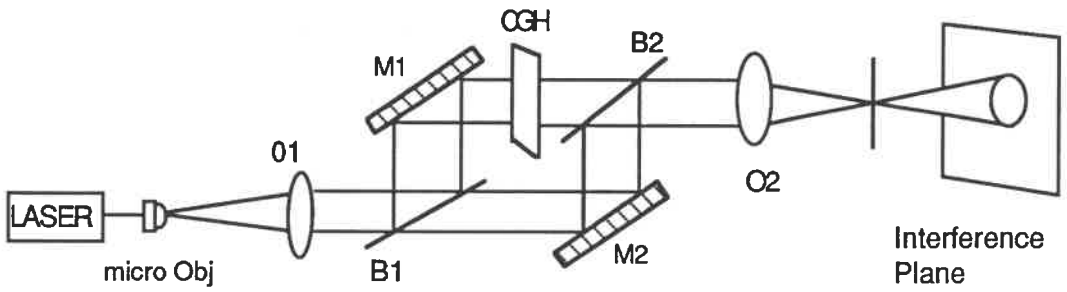


Fig. 13. Arrangement to analysis the wavefront of CGHs

We use the MZI because this interferometer permits to test samples in transmission and in one single pass.

In figure 13, the CGH is shown in one arm of the interferometer, where $B_i$ are beam splitters, $M_i$ are mirrors and $O_i$ are objective lenses. It is positioned so that its image and the reference beam coincide. We put a filtering aperture in the focal plane of the objective lens $O_2$, to elliminate some noise.

The wavefront error (aberration) is measured as the difference between the aberrated wavefront and the reference wave (plane wave).

The CGHs present the correct quantities of aberrations.

# C2: Set-up used to Record HOEs

After we had checked the quality of the CGH we began the preparation of the set-up for recording the HOEs with aberrated reference wavefront and with the nonaberrated wavefront (CGH only with carrier).

Figure 14, shows the experimental set-up used to record the different HOEs (see also fig. 15).

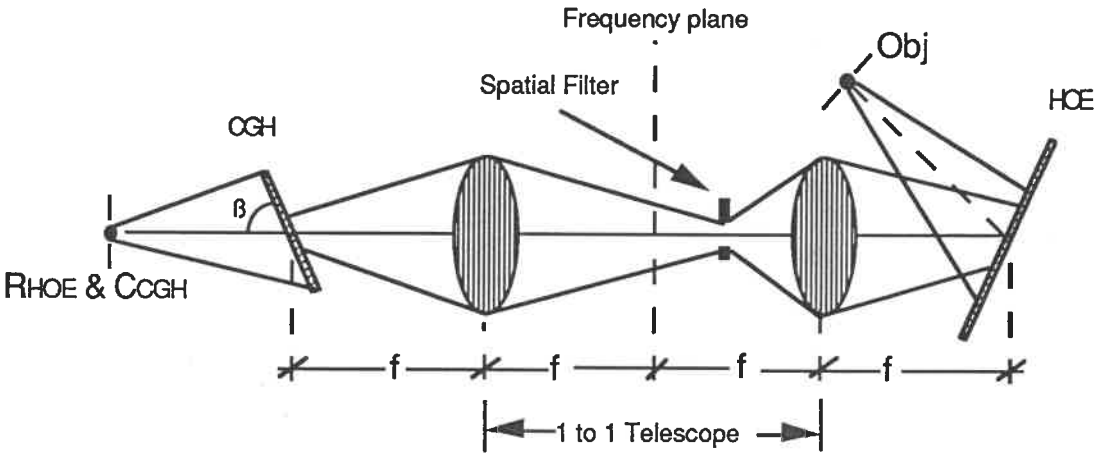


Fig. 14. The HOE recording geometry used to record the HOEs using a CGH

In this phase different HOEs were recorded. For each kind of aberration we recorded a HOE using a CGH that transformed the spherical reference wave into an aberrated wave and also a HOE using a CGH that only added some tilt to the reference wave.

In all cases we recorded one HOE using the +1 and another using the -1 diffraction orders as reference wave.

The diffracted wavefront from the CGH is reimaged at the HOE recording plane by a one-to-one telescope. This telescope does not only perform imaging from the CGH plane to the HOE plane, but also preserves the desired phase relationships, i.e., it does not introduce an extra spherical phase term as would appear in imaging with a single lens.

An objective and a pinhole assembly provides the required object point source and reference point source.

The tilt of the CGH and HOE is such that the desired offset angles are obtained at the readout and recording planes, and that CGH and HOE are in conjugate image planes. It is necessary to be careful in this phase of the experiment, to assure these conditions.

A spatial filter is positionned at the frequency plane such that only the desired first-order diffracted wavefront of the CGH is passed to the recording plane.

The experimental parameters for Spherical Aberrations (S) are $Rc=Ro=\infty$, $Ri=Rr$, $xi=+xr$ and $\lambda c \neq \lambda r$. We took

$\lambda c=0.6328\ \mu m$, $\lambda r=0.5145\ \mu m$, $zr=5$ cm and $xr=1$ cm ($ß=\text{arctn}(\frac{1}{5})$);

For Coma (C) the parameters are $Ro=Rr$, $Ri=\infty$, $Rc=\infty$, $xo=-xr$ and $\lambda r=\lambda c$, with

$\lambda r=0.5145\ \mu m$, $zr=20$ cm and $xr=5$ cm ($ß=\text{arctn}(\frac{5}{20})$);

For Astigmatism (A), we have $Ro=Rr=Rc=Ri$, $xc=0$, $xr=-xo$, $xi=\pm 2xr$ and $\lambda r=\lambda c$, and made

$zr=20$ cm, $xr=5$ cm ($ß=\text{arctn}(\frac{5}{20})$) and $\lambda r=0.5145\ \mu m$,

where $Rj=\sqrt{xj^2+zj^2}$.

In order to obtain a comparison based on the correction of HOE aberration, we decided to record the correct HOE and uncorrected HOE in the same conditions, and use the same set up.

The plates used to record the HOEs were 8E56HD Holotest Plates from Agfa Geveart. These plates have high resolution, 3000 lin/mm.

In the appendix E3 we describe all steps of the development and the used solutions.

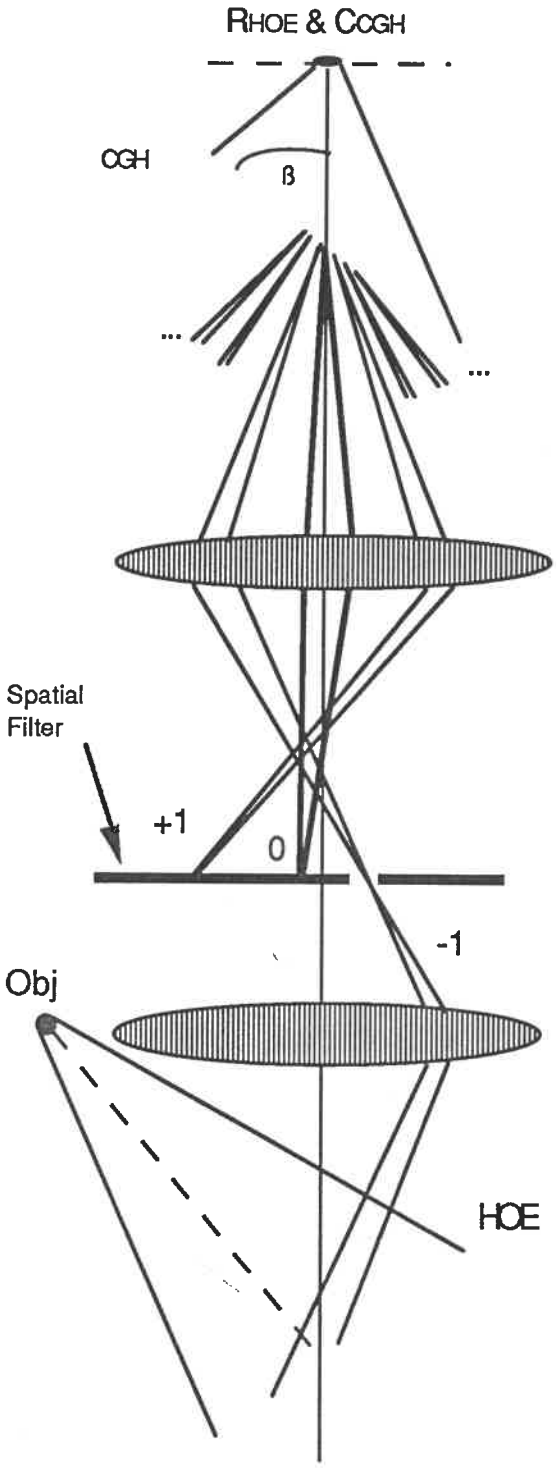


Fig.15. Schematic diagram of the set-up used to record the HOEs, where the zero, +1 and -1 diffraction orders are shown .

# C3: Set-up used to Analyze HOEs

1. Coma
2. Astigmatism
3. Spherical Aberration

## 1. Coma

In order to analysis the wavefront produced by HOEs(coma) (HOEs in the case of coma), their reconstructions were interfered with a plane wave, using the arrangement shown in figure 16 (Mach-Zehnder Interferometer).

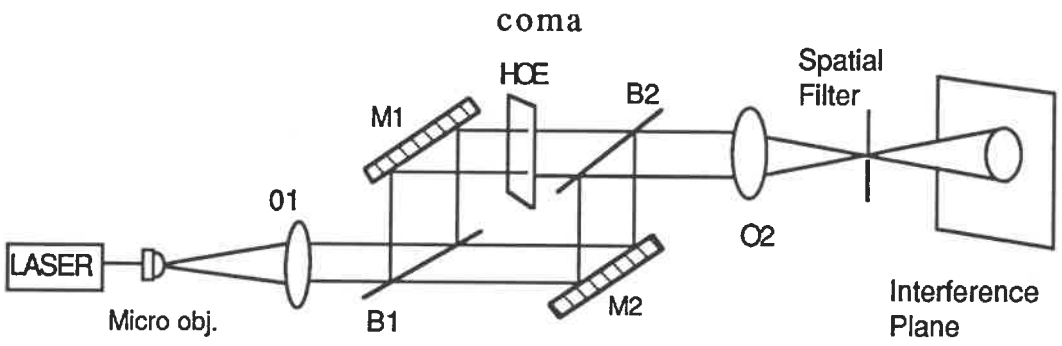


Fig. 16. Arrangement used to analysis the wavefront of HOEs

The conditions for obtaining only coma, as we saw at §A2 (page 17), are:

$$Ro=Rr,\ xo=-xr,\ \text{and}\ Rc=\infty$$

So, we must read these HOEs with a plane wave. The same conditions yield $Ri=\infty$ for the position of the image. In reality, we had not a plane wave, which made the analysis of this kind of HOEs difficult.

In all cases we analysed the two first-orders of the HOEs. For each kind of HOEs we made the comparison between the pattern obtained with the corrected and noncorrected HOEs.

## 2. Astigmatism

To analysis the wavefront produced by HOEs(Ast), we used a set-up similar to that used to analysis the HOEs(coma), with small differences, as shown in fig. 17.

These differences are determined by the conditions to obtain Astigmatism, which are: Ro=Rr=Ri=Rc and xc=0.

We must read these HOEs with a spherical wave with the same characteristics xc=0 and Rc=Ro.

As the images are spherical waves it is necessary to collimate these waves, which was not trivial.

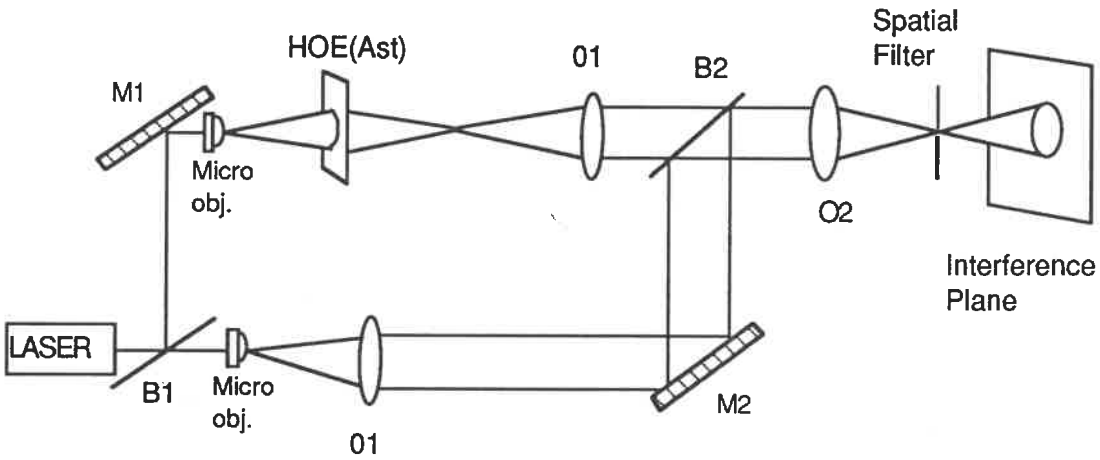


Fig. 17. Arrangement for the analysis of the HOEs(ast)

## 3. Spherical Aberrations

Now we must use a plane wave to read the HOEs(S.ab.), and collimate the imagewave, in agreement with the conditions needed to obtain Spherical Aberration, which are:

$$Rc=\infty \text{ and } Ri=Rr \text{ and } \lambda c=0.6328\ \mu m$$

For the analysis of these HOEs(S.ab.), the set-up shown in fig. 18 was used.

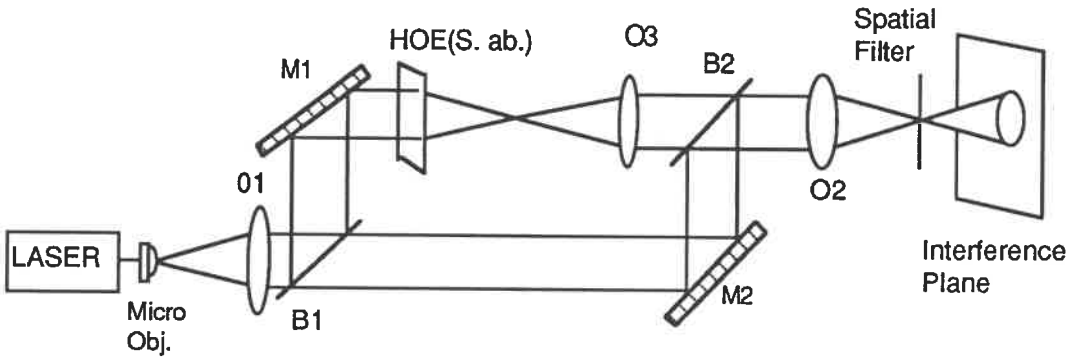


Fig. 18. Arrangement for analysis of HOEs(S. ab.)

# Parte III: Results and Conclusion

## D1: Results discussion, conclusion and recommendation

The initial analysis of the different HOEs recorded didn't show significative differences among the patterns obtained with the corrected HOEs and the patterns obtained with the noncorrected HOEs.

After that, we checked and revised all processes and we recorded another set of HOEs, but when we analysed this new set of HOEs we didn't see appreciable difference among their patterns. It is highly, probable that we committe in the process, a systematic error.

As we already had recorded more than thirty HOEs we stoped all experimental work and began to look for alternative methods.

We found another method to the one we used. This method was proposed by Y. Amitai and A. A. Friesem[20,...,29], who refer that the other method is more reliable and less complex.

The authors of these papers suggest to use a intermediate optical hologram (OH) instead of a CGH, i.e., recording wavefronts used are generated by OHs and/or COEs.

We think it would be a good idea to repeat the process using the method of Y. Amitai and A. A. Friesem.

Unfortunately, the time destinated for this work (3 months) was too short to start a new method.

# References

1. D. H. Close, "Holographic Optical Elements", Opt. Eng. 14, 408 (1975)

2. Reynolds, DeVelis, Parrent, Thompson, "The New Physical Optics Notebook: Tutorials in Fourier Optics", SPIE Optical Enginneering Press, New York (1989)

3. K. A. Winick and J. R. Fienup, "Optimum holographic elements recorded with nonspherical wave fronts", J. O. S. A. 73, 208 (1983)

4. R. Rallison, "Applications of Holographic Optical Elements", Lasers & Applications, December 1984

5. J. Kedmi and A. A. Friesem, " Optimized holographic optical elements", J. O. S. A. A 3, 699 (1986)

6. J. M. Tedesco and R. C. Fairchild, "Design and fabrication of aspheric holographic optical elements", SPIE Vol. 532, 277 Applications of Holography (1985)

7. Robert. D. Guenther, "Modern Optics", John Wiley & Sons, Inc. (1990)

8. R. W. Meier, "Magnification and Third-Order Aberrations in Holography", J. O. S. A. 55, 987 (1965)

9. E. B. Champagne, "Nonparaxial Imaging, Magnification, and Aberration Properties in Holography", J. O. S. A. 57, 51 (1967)

10. J. N. Latta, "Computer-Based Analysis of Hologram Imagery and aberrations I: Hologram Types and Their Nonchromatic aberrations", Appl. Opt. 10, 599 (1971)

11. J. N. Latta, "Computer-Based Analysis of Hologram Imagery and aberrations II: Aberrations induced by a Wavelength shift", Appl. Opt. 10, 609 (1971)

12. J. N. Latta, "Computer-Based Analysis of Holography Using Ray Tracing", Appl. Opt. 10, 2698 (1971)

13. Y. Ishii, J. Maeda and K. Murata, "Holographic display of diffraction patterns suffering from third-and fifth-order aberrations", Optica acta 26, 969 (1979)

14. S. Roose, "Project: Correction of aberrations with a CGH.", ALNA-TW-VUB, Pleinlaan 2, B-1050 Brussels, Belgium

15. R. C. Fairchild, J. R. Fienup, "Computer-originated aspheric holographic optical elements", Opt. Eng. 21, 133 (1982)

16. C. S. Ih, L. Q. Xiang, And C. W. Yang, " Making an ir HOE Using a CGH", SPIE Vol. 1136 Holographic Optics II: Principles and Applications (1989)

17. A. J. Lee and David P. Casasent, "Computer generated hologram recording using a laser printer", Appl. Opt. 26, 136 (1987)

18. M. A. A. de Sousa, "Erasmus Program-Report", VUB/UP (1990)

19. James C. Wyant, "Optical Testing and Testing Instrumentation", Optical Sciences Center, University of Arizona and WYKO Corporation Tucson, Arizona, 1987

20. J. Kedmi and A. A. Friesem, " Optimal holographic Fourier-transform lens", Appl. Opt. 23, 4015 (1984)

21. J. N. Cederquist and J. R. Fienup, " Analytic design of optimum holographic optical elements", J. O. S. A. A 4, 699 (1987)

22. H. Chen, R. R. Hershey, and E. N. Leith, " Design of a holographic lens for the infrared", Appl. Opt. 26, 1983 (1987)

23. T. Shiozawa and H. Iwaoka, "Analysis of a low-aberration holographic scanner", Appl. OPt. 27, 1992 (1988)

24. Y. Amitai and A. A. Friesem, "Design of holographic optical elements by using recursive techniques", J. O. S. A. a 5, 702 (1988)

25. Y. Amitai and A. A. Friesem, "Combining low aberrations and hogh diffraction efficiency in holographic optical elements", Optics Letters 13, 883(1988)

26. M. Assenheimer, Y. Amitai, and A. A. Friesem, "Recursive design for an efficient HOE with different recording and readout wavelengths", Appl. Opt. 27, 4747 (1988)

27. Y. Amitai, A. A. Friesem, and V. Weiss, "Holographic elements with high efficiency and low aberrations for helmet displays"",Appl. Opt. 28, 3405(1989)

28. Y. Amitai, A. A. Friesem, and V. Weiss, "Designing holographic lenses with different recording and readout wavelengths", J. O. S. A. A 7, 80 (1990)

29. K. Goto and A. Terasawa, "Analytical design of holographic optical elements for Fourier transfom", J. O. S. A. A 7, 2109 (1990)

30. Joseph W. Goodman, "Introduction to Fourier Optics", McGraw-Hill, Inc. (1968)

31. W. T. Cathey, "Optical Information Processing and Holography", John Wiley & Sons, Inc. (1974)

32. M. Born and E. Wolf, "Principles of Optics", Pergamon Press, New York (1964)

33. W. H. Lee, "Computer-Generated Hologram: Principles and Applications", Progress in Optics, 121-229,

34. S. Roose, "Computer-generated hologrphy: The state of the art.", Internal report (1988-1989), ALNA-TW, VUB, Pleinlann 2, B-1050 Brussels, Belgium

35. B. R. Brown and A. W. Lohmann, "Complex Spatial Filtering with Binary Masks", Appl. Opt. 5, 967 (1966)

36. A. W. Lohmann and D. P. Paris, " Binary Fraunhofer Holograms, Generated by Computer", Appl. Opt. 6, 1739 (1967)

37. G. Tricoles, "Computer generated holography: an historical review", Appl. Opt. 26,4351 (1987)

38. Serge Habraken, "Hologrammes Générés par Ordinateur: Techniques de Copiage de Masques Binaires", Mémoire présenté en vue de l'obtention du grade de Maître en Physique: Optoélectronique, Université de Liège (1990-1991)

39. S. Roose, E. Stijns, "Realization of CGHOEs for optical pattern recognition.", ALNA-TW, VUB, Pleinlann 2, B-1050 Brussels, Belgium

40. A. W. Lohmann, "How to make Computer Holograms", To be presented at the SPIE seminar "Holography'71", Boston, April 14-15, 1971

41. J. D. Gaskill, "Linear Systems, Fourier Transforms and Optics", John Wiley and Sons, Inc., New York (1978)

42. W. H. Lee, "Binary Synthetic Holograms", Appl. Opt. 13, 1977 (1974)

43. M. Françon,"Optical Interferometry", Academic Press Inc. (1966)

# Appendixes

E1: **A Serie of Interferograms Patterns with Aberrations**

E2: **Millimask Plates HD 59380FL5 AGFA GEVEAERT**

E3: **Processing of "Holotest" Plates 8E 56HD**

# E1: A Serie of Interferograms Patterns with Aberrations

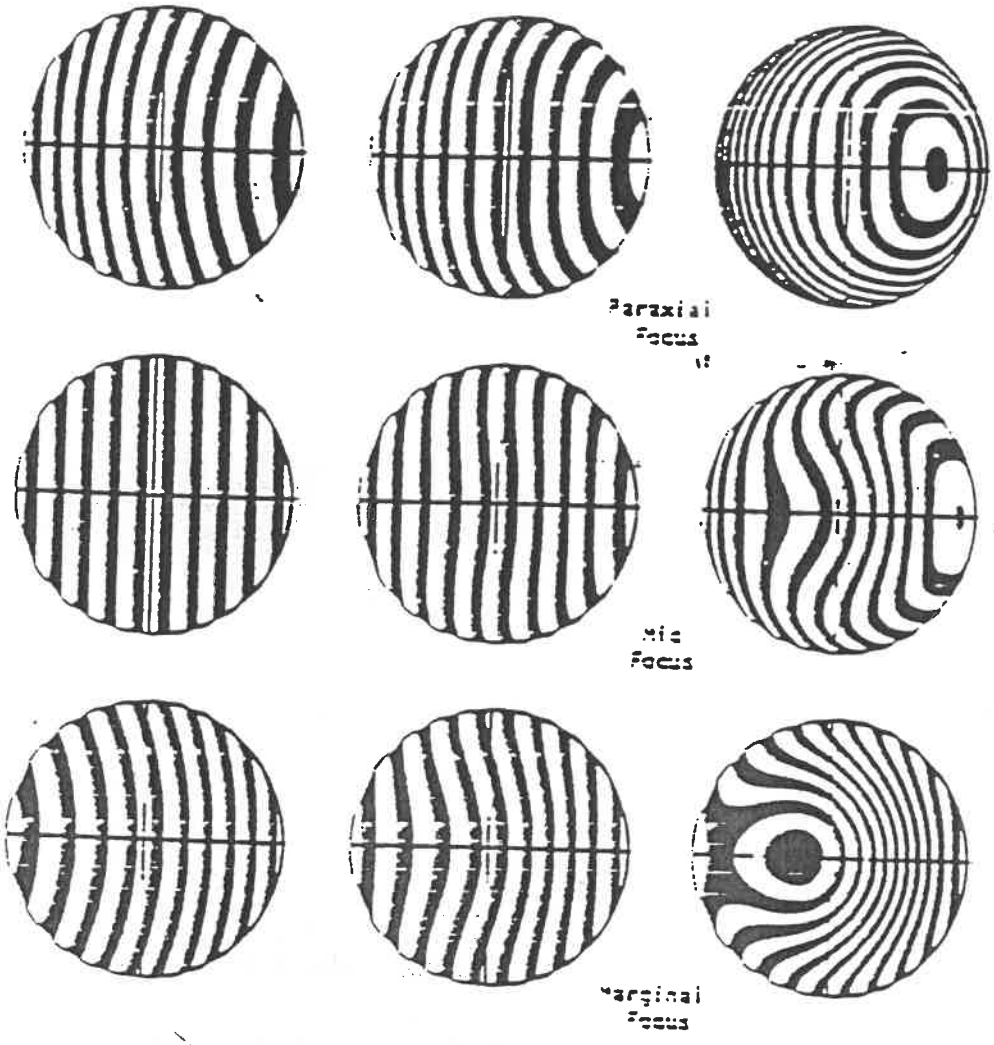


spherical aberration.

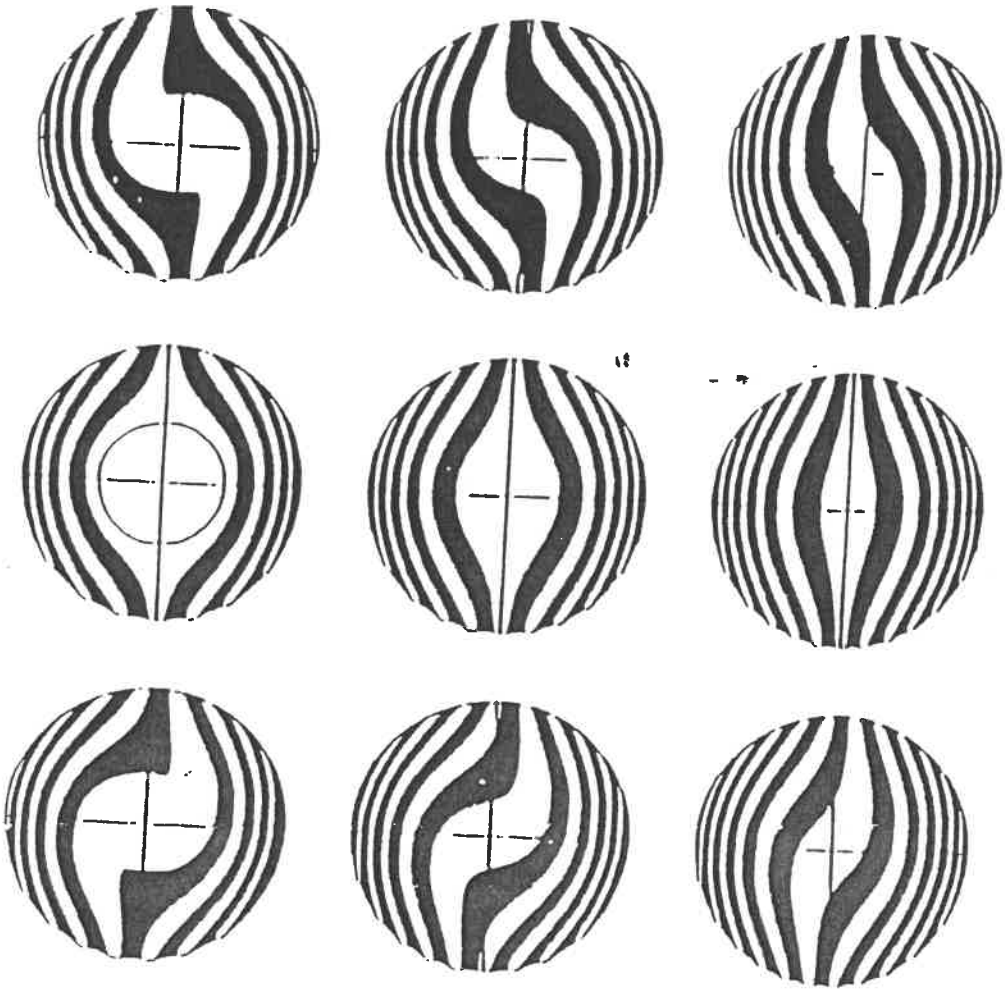

large coma. small tilt.

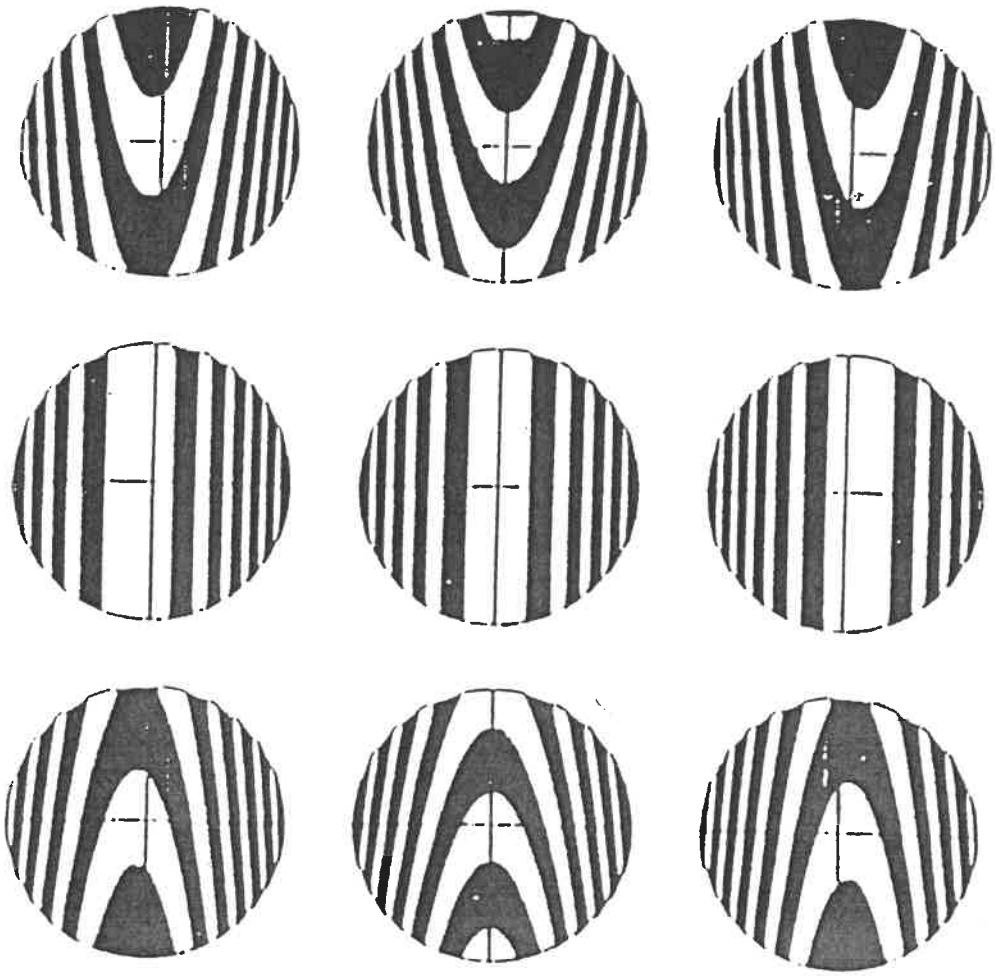

large astigmatism,
sagittal focus, small tilt.

## E2. Millimask Plates HD 59380FL5 AGFA GEVEAERT

# Instructions for use for processing MILLIMASK Plates

HD 593807 FL 5

## 1. Negative processing

| | |
|---|---|
| 4 min | Development in G 282 c (1 + 4) |
| 2 min | Rinse in D.I. water |
| 2 min | Fixation in G 333 c (1 + 4) |
| 10 min | Rinse in D.I. water |
| | DRY |

N.B. All chemicals at 21 °C ± 0.5 °C

→ - STOP THE DEVELOPMENT: ACETIC ACIDE 96% EXTRA PURE (1 + 20 PARTS of WATER), 2 min
- RINSE IN WATER

## 2. Reversal processing

**For contact**

| | |
|---|---|
| 3-4 min | Development in G 283 |
| 2 min | Bleach A-G formula |
| 3 min | Clear A-G formula |
| 2 min | Rinse in D.I. water with 1 min reversal exposure |
| 1 min | Development Agfa G 282 c (1 + 2) |
| | or (1 + 4) |
| 2 min | Fixation in G 333 c (1 + 4) |
| 10 min | Rinse in D.I. water |

N.B. Rinse 2 min in D.I. water between each step
All chemicals at 22 °C ± 0.5 °C

## 3. HD reversal processing (high speed)

**For pattern generator or/and Step-and-Repeat camera**

| | |
|---|---|
| 2 min | Development in G 284 c (1 + 3) |
| 2 min | Development in G 283 |
| 2 min | Clear A-G formula |
| 2 min | Bleach A-G formula |
| 3 min | Clear A-G formula |
| 2 min | Rinse in D.I. water with 1 min reversal exposure |

N.B. Further as mentioned above reversal processing for contact

## 4. COPYLINE HDP plates

| | |
|---|---|
| **Development** | Tray processing at 20 °C<br>G 101 c 2 min |
| **Rinse** | 2 min in running water at 20 °C |
| **Fixation** | G 333 c 2 min |
| **Rinse** | 10 min in running water at 20 °C |

## E 3 . Processing of "Holotest" Plates 8E 56HD

Holographic "Holotest" Plates 8E 56 HD have the sensibilization energy (E) about 50 $\mu J/cm^2$ at D $\approx$ 2. The range of sensibility of this plates is 350 to 560 nm, the esposure time is given $E/(W/cm^2)$, where W is the total optical power at the hologram plane.

For a good diffraction efficiency the ratio between the optical power of the object and the reference must be near 1 at the hologram plane.

The method utilized at V.U.B. for processing "Holotest" Plates 8E 56 HD is a modification of the "Van Renesse" Method.

## Procedure

1) Development, hardening nº1: bath nº1: 2 min.
2) Rinse in water: 30 sec.
3) Hardening nº2, bleach nº1, fix nº1: bath nº2 till clear
4) Rinse in water: 30 sec.
5) Bleach nº2, fix nº2, bath nº3: 3 min.
6) Rinse in water energetically: 30 sec.
7) Stream hot air
8) Wait half an hour for partial color recovery

## Baths Compositions

Before each set of developments is necessary to prepare new baths.

### Bath nº1

Stock A: 5 g Pyrogallol

0.5 l water

Stock B: 30 g Nitrium Carbonato-sodium Carbonate ($Na_2CO_3$)
0.5 l water

Mix A and B just before use: **no conservation of the mixture!**

Bath nº2

Stock A: 0.5 cc Sulfuric Acid $H_2SO_4$
1 l water

Stock B: 3 g Ammonium Bichromate $(NH_4)_2Cr_2O_7$

Mix powder B in solution A before use: conserve maximum 12 hours after mixing!

Bath nº3

Stock A: 10 cc Sulfuric Acid
1 l water

Stock B: 0.8 g $KMnO_4$

Mix powder B in solution A before use: conserve maximum 12 hours after mixing!

## 2 AMPLITUDEHOLOGRAFIE

### 2.1 Densiteits- en amplitudetransmissiecurven

Het verband tussen de densiteit D en de belichting E wordt in het algemeen voorgesteld door middel van de karakteristieke curve. De karakteristieke curven van de Holotest-emulsies 8 E 75 HD en 10 E 75 (voor rood laserlicht) en 8 E 56 HD en 10 E 56 (voor blauw en groen laserlicht) worden in fig. 1 gegeven.

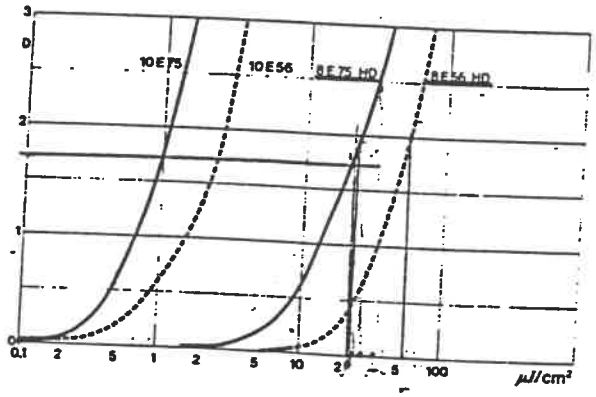


fig. 1

De belichtingen voor Holotest 8 E 75 HD en 10 E 75 werden uitgevoerd bij 627 nm en voor 8 E 56 HD en 10 E 56 bij 514 nm.
Er werd ontwikkeld in G 282 (1 + 2) gedurende 4 minuten bij 20 °C. Na tussenspoelen in water (1 minuut bij 20 °C) werd gefixeerd in Agfa-Gevaert-fixeerbad G 321 gedurende 4 minuten. Daarna werd 15 minuten gespoeld.
De densiteit van de ontwikkelde emulsielagen werd in parallel licht gemeten. De karakteristieke curven zijn voor bepaalde holografische opnamen een bruikbare informatie, maar meestal wordt de voorkeur gegeven aan de amplitudetransmissiecurven. Een hologram werkt immers als een buigingsrooster ten opzichte van het invallend golffront, waarbij niet de plaatselijke zwarting, maar de plaatselijke amplitudetransmissie de belangrijkste rol speelt. De amplitudetransmissie wordt gedefinieerd als de verhouding tussen de amplitude van een monochromatische vlakke golf na en voor de doorgang doorheen de fotografische laag. Zij is in het algemeen een complexe grootheid, m.a.w. de invallende straling wordt niet alleen in amplitude maar ook in fase beïnvloed. Bij ontwikkelde emulsies is echter alléén de intensiteitstransmissie $T_i = T_a T_a^*$ (waarbij $T_a^*$ de toegevoegd complexe waarde van $T_a$ is) een gemakkelijk te meten grootheid, waaruit men de grootte van de amplitudetransmissie $|T_a|$ verkrijgt. Deze grootheid wordt in functie van de belichting voor de Holotest 8 E 75- HD en 10 E 75-emulsies bij een golflengte $\lambda = 627$ nm, en voor de Holotest 8 E 56- en 10 E 56-emulsies bij een golflengte $\lambda = 514$ nm in fig. 2 gegeven.
De met $|T_a| = 0{,}5$ overeenstemmende energie per eenheid van oppervlakte kan als een aanduiding voor de gevoeligheid gelden: De lichtintensiteiten voor $|T_a| = 0{,}5$ (dit stemt overeen met D = 0,6) bedragen :

~ 0,5 μJ/cm² voor 10 E 75
~ 10 μJ/cm² voor 8 E 75 HD
~ 1 μJ/cm² voor 10 E 56
~ 25 μJ/cm² voor 8 E 56 HD

Deze waarden worden ook enigszins beïnvloed door de ontwikkelomstandigheden.

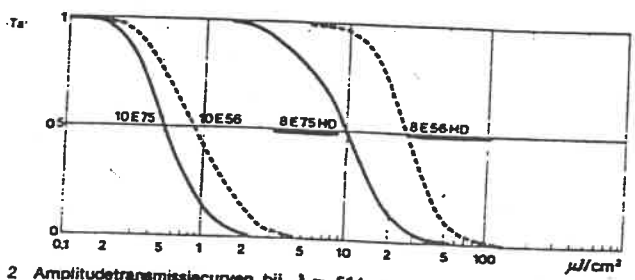


fig. 2 Amplitudetransmissiecurven bij λ = 514 nm - - - -
λ = 627 nm ——
Ontw. G 282 c (1 + 2) - 4 min - 20 °C

## 2.2 Spectrale gevoeligheid

De holografische emulsies Holotest 8 E 75 HD en 10 E 75 zijn speciaal sensibiliseerd voor het golflengtegebied van 600 - 750 nm, met het oog het gebruik met de He-Ne-laser (633 nm) en de robijnlaser (694 r Daarentegen zijn de holografische emulsies Holotest 8 E 56 HD en 10 E geschikt voor opnamen met golflengten tot 560 nm (krypton-, argonlas

De in hoofdstuk 2.1 opgegeven densiteits- en amplitudetransmissiecur zijn toepasselijk op de golflengte resp. van de He-Ne-laser ($\lambda = 633$ r en de kryptonlaser (476 nm en 521 nm). Om de omrekening van de beli ting naar andere golflengten mogelijk te maken, worden de spectrale voeligheden in fig. 3 gegeven.

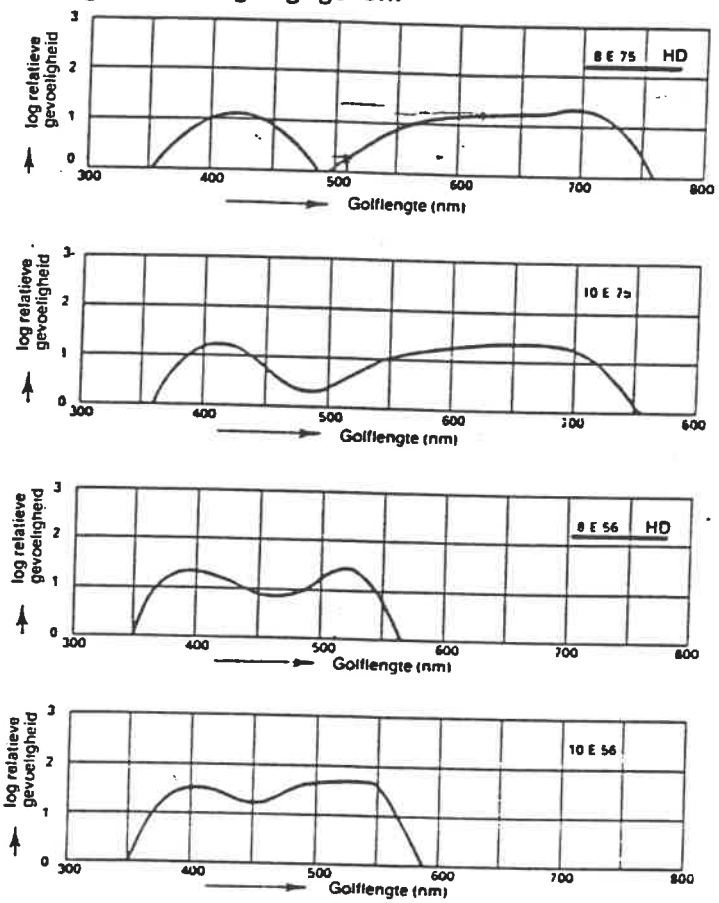


fig. 3 Spectrale gevoeligheid bij een equi-energetisch spectrum

## 2.3 Beeldkwaliteit

Om de beeldkwaliteit van de holografische emulsie te bepalen werd ee optische diffractiemethode gebruikt. Hierbij werd een twee-straalinte ferentie-belichting toegepast en het aldus verkregen buigingsroost gemeten. Het schema der belichting en reconstructie wordt in fig. gegeven.

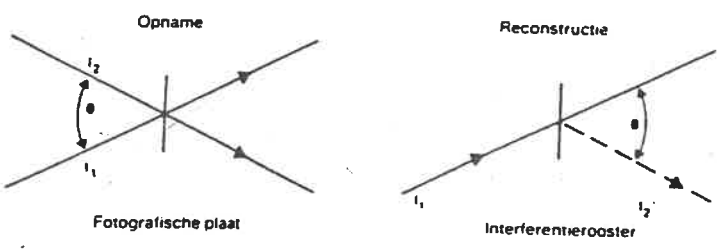


fig. 4 Schema van de opname en reconstructie van tweestraal-interferenties

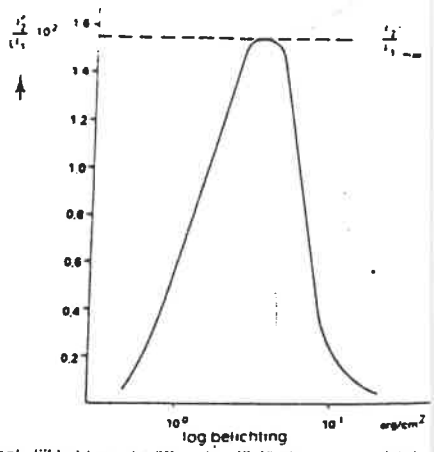


fig. 5 Afhankelijkheid van de diffractie-efficiëntie van de belichtin